THE BOUNDARY CONDITION AT THE MOVING SHORELINE FOR NEARSHORE MODELS

by

Ravi S. Prasad

and

Ib A. Svendsen

RESEARCH REPORT NO. CACR-01-02
April 2001

CENTER FOR APPLIED COASTAL RESEARCH
Ocean Engineering Laboratory
University of Delaware
Newark, Delaware 19716

TABLE OF CONTENTS

ABSTRACT

One of the most important problems faced when modeling nearshore flows is to establish an appropriate representation at the shoreward boundary of the domain. Depth integration is used in some nearshore models to reduce complete 3D governing equations to 2DH and this provides excellent results for nearshore currents. However, at the shoreline, as the waterdepth goes to zero, this gives the trivial zero-solution. A related approach is used in Boussinesq theory where the solution establishes a polynomial approximation to the vertical velocity profile which leads to similar 2DH equations. In both the cases, however, the moving shoreline changes the position where a condition of zero waterdepth and volume flux has to be imposed.

Another aspect of the moving shoreline boundary problem is that the motion of the shoreline results in a time varying fluid domain which is to be modeled numerically, as the offshore boundary of the region of interest remains fixed.

In the past, this problem has essentially been treated with either fixed grid methods or with co-ordinate transformation methods. In the fixed grid methods, the computational grid points remain at constant position and the status of some grid points change from wet to dry and vice-versa as the shoreline moves. In the previous attempts with fixed grid methods the shoreline position between the last wet and the first dry point is either not calculated or is obtained by some extrapolation method. The transformation methods can be selected so that a high resolution can be obtained in the region where it is necessary and thus can provide a more accurate results at a less computational cost.

In the present work, the equations for the shoreline motion have been developed and a time varying fluid domain has been implemented in the numerical scheme using a co-ordinate transformation and a fixed grid method with a wet-dry interface. It has been shown that the problem here essentially is to find the velocity and the position of the shoreline. Once they are known, a numerical scheme can easily be developed to incorporate a time varying model domain.

The results are presented in comparison with the analytical results in 1DH and with the numerical results from other models in 2DH cases. It was found out that the accuracy of the results depends very much on the grid spacing. An increase in the time step doesn't produce a large error in the numerical solution.

The transformation method which appears to be more advantageous, can only be applied efficiently in the cases where a predominant shoreline exists. In other cases, such as modeling of bays and embayments, fixed grid method seems more suitable.

Chapter 1

INTRODUCTION

One of the most important problems faced when modeling nearshore flows is to establish an appropriate representation at the shoreward boundary of the domain. Depth integration, which is used in all the nearshore models to reduce complete 3D governing equations to 2DH, provides excellent results in the nearshore. However, as the waterdepth goes to zero at the shoreline, this gives the trivial zero-solution. This means that the equations used inside the computational domain degenerate to zero at the shoreline. The fluxes, which are velocities integrated over the depth, become zero at the shoreline, but this doesn't necessarily imply that the particle velocity at the shoreline will become zero. In the shallow water region, where the fluid velocity is fairly uniform over depth, velocities can be calculated by dividing the fluxes by the waterdepth. This, however, can't be done at the shoreline, and this results in the necessity to derive a new equation for the motion of the shoreline itself.

A related approach is used in Boussinesq theory where the solution establishes a polynomial approximation to the vertical velocity profile which leads to similar 2DH equations.

The non-zero particle velocity at the shoreline, changes the shoreline position with time. So, the point where the volume fluxes are zero, changes it's spatial position, which results in a time varying fluid domain, which is to be modeled in the numerical computations.

So the problem at hand can essentially be divided into two parts, first to develop a description for the velocity of the shoreline and thus the changes in the shoreline position with time and second to devise a method to incorporate a time varying model domain in the numerical scheme.

The simplest boundary condition that can be applied at the shoreward boundary of a model domain is to use a wall boundary condition at the initial shoreline. Under this condition, the shoreline doesn't move with time and the fluxes at the initial shoreline are always zero. As shown by Lynch and Gray (1980), this type of shoreline boundary condition doesn't affect the results even a moderate distance from the boundary very much, but near the boundary, it may result in significant errors.

Near the shoreline, flow properties change rapidly with the cross-shore distance. A significant amount of sediment transport also occurs in the neighborhood of the shoreline. In order to be able to predict these processes and the flow in the swash region, an accurate and efficient model for the treatment of the shoreline is required.

In the past, the time varying fluid domain has been modeled in Eulerian schemes essentially using either a wet-dry interface for the shoreline with fixed grids or a coordinate transformation, where the instantaneous model domain is transformed onto a fixed, evenly spaced, rectangular computational grid. These options are discussed in more detail below.

With the use of Lagrangian description, moving boundaries can be treated efficiently. Some examples of this are presented in Pedersen and Gjevik (1983), Zelt and Raichlen (1990) and Zelt (1991).

Brocchini and Peregrine (1996) suggest different ways of analyzing the mean shoreline for wave averaged models and outline a method of treatment of the moving shoreline for such models as the lower edge of the swash by using the integral flow

properties of the swash zone.

In the present work, the governing equations for the nearshore circulation model SHORECIRC will be used to describe the nearshore flow. The dispersive and dissipative terms in these equations will be treated as source terms to the nonlinear shallow water equations and will be disregarded in this work. The Boussinesq equations can also be regarded as the nonlinear shallow water equations in which the dispersive terms essentially are treated as inhomogeneous source terms.

1.1 Fixed grid methods

Due to it's conceptual simplicity, many numerical models use fixed grids with a wet-dry interface to treat the moving shoreline. Reid and Bodine (1968) were among the first to use this type of model at the shoreline. They used this scheme in their storm surge model. The bottom elevation was assumed to be constant over a grid and thus the actual topography was approximated by a stair-step like topography. The flux through the last wet grid to the first dry grid was given by an empirical relation which was a function of the height of the water column in the wet grid above the land elevation in the dry grid. Hibberd and Peregrine (1979) used a fixed grid method to describe the run-up and run-down of a uniform bore on a plane sloping beach. Here linear extrapolation was used to determine the waterdepth and the velocity at the first dry grid point during run-up. If the waterdepth at the first dry grid point was greater than a threshold value, it was included in the computational domain. During run-down, the last wet point was excluded from the computational domain when the waterdepth there goes below that threshold value. Kobayashi *et al.* (1987) used a similar method in their model. Militello (1998) describes a method of flooding and drying of grid cells for a model on staggered grids. In this scheme, a wet cell becomes dry when the waterdepth at the center of that cell gets smaller than a specified "critical" depth, and a dry cell becomes wet when at least one of the four adjacent cells have a surface elevation higher

than the bottom depth at the dry point together with the flow at the corresponding boundary of these two cells, is in the direction of the dry cell. Liu *et al.* (1995) declares the first dry point to become wet when the surface elevation at the last wet point becomes greater than the bottom elevation at the first dry point and the surface elevation at the newly wet point is assigned the same surface elevation as at the last wet point. In all these methods described above, the actual shoreline position is never identified. Balzano (1998) compares many wet-dry methods and proposes some new methods of it's implementation in the models for tidal flooding. These methods had slightly different criterion for declaration of a grid to become wet or dry and they also differed in the method to calculate the volume of water left in a grid when it was declared dry. However, none of the methods discussed here, determines the shoreline position between the last wet and the first dry grids.

Sielecki and Wurtele (1970) and VanDongeren and Svendsen (1997b) are among others who used a wet-dry interface on fixed grids to model a moving shoreline and tried to determine the actual shoreline position. Sielecki and Wurtele (1970) determines the shoreline position between the last wet and the first dry grid points, but this is done by using a linear extrapolation to the shoreline of the surface elevation and velocity from the neighboring wet points. VanDongeren and Svendsen (1997b) used the method of volume of water stored past the last wet point and assumed a triangular shape of that to estimate the actual shoreline position, and when the distance of the shoreline from the last wet point becomes more than a grid spacing, the first dry grid point was declared wet and was included in the calculations at the next time steps. Similarly when this distance becomes less than zero, the last wet point is excluded from the computational domain at the next time steps.

In a fixed grid, the shoreline position will generally fall between two grid points, the last wet and the first dry point going shoreward. The lack of information

about the shoreline position between the last wet and the first dry grid points makes the declaration of a grid to be wet or dry difficult. Because there are no flow values at the dry points simple interpolation is not possible. In some cases of implementation with fixed grid, e.g. Reid and Bodine (1968), Militello (1998) etc. , only regular grid points are chosen as shoreline points, which means that the shoreline is moved one or more Δx at a time. This makes the wetting and drying procedure more impulsive and can be one of the reasons that makes wet-dry methods more prone to numerical instabilities.

In the fixed grid method described in chapter (5) below, the position of the shoreline is determined as a special point positioned between the last wet and the first dry grid point. This is done by solving the momentum equation for a fluid particle at the shoreline.

1.2 Use of a coordinate transformation

The other category of methods for treatment of the moving shoreline, which have been described in the literature is the use of a coordinate transformation. In this method the real, time varying physical domain is transformed onto a time invariant, computational domain. At any instant of time, the computational domain corresponds to the real domain at that time. As the moving shoreline changes the cross-shore length of the domain, most of the coordinate transformation schemes used to model this, changes the grid spacing only in the cross-shore direction. All the coordinate transformation methods assume that the shoreline position at any given time, is a single valued function of the longshore position.

The simplest type of coordinate transformation scheme to achieve this goal was the one used by Johns (1982), where the cross-shore coordinate x is transformed to X using a transformation similar to,

$$X = \frac{x}{L(t)} \tag{1.1}$$

where x is measured from the fixed offshore boundary and $L(t)$ is the length of the real domain at time t. This results in a linear mapping of the time varying real domain $x = [0, L(t)]$ to the fixed computational domain $X = [0, 1]$. Johns *et al.* (1982) describe a similar approach of coordinate transformation for the modeling of storm surges on the east coast of India. Shi and Sun (1995) describe a coordinate transformation method that takes into account the time varying shoreline in their finite difference model for storm surge in the generalized curvilinear coordinate. In all these methods not only do the horizontal coordinates get transformed but also the velocities get modified so that the modified velocity in the transformed plane is zero.

Jamet and Bonnerot (1975), Lynch and Gray (1980), Gopalakrishnan and Tung (1983) describe a few examples of implementation of a transformation method in finite element models. Jamet and Bonnerot (1975) and Lynch and Gray (1980) used continuously deforming finite elements where the last element followed the fluid boundary. Gopalakrishnan and Tung (1983) used Lagrangian acceleration to find the motion of the shoreline and a variable element length. In this method, the motion of the shoreline increases the length of the last element. When this length becomes larger than 1.2 times the initial element length, the last element splits into two parts. The paper describes the numerical scheme and shows an example of run-up. However, it doesn't describe or show examples of run-down.

Özkan Haller and Kirby (1997) used a shoreline transformation technique to take into account the moving shoreline in their spectral collocation model for nearshore circulation. Here the coordinate transformation was done in two steps. In the first step the time varying fluid domain was transformed onto a fixed domain which was then transformed again so that the image domain becomes [-1,1]. The second transformation was required because of the use of Chebyshev collocation method to calculate spatial derivatives in the cross-shore direction. As described here, the

coordinate transformation method can be modified to obtain smaller grid spacing in the region where a higher resolution is required than the rest of the domain. In modeling a moving shoreline, a high resolution is required near the shoreline where the flow properties change more rapidly with spatial distance. However this effect is included in the second transformation and hence can't be used with other numerical schemes.

The advantage of this type of shoreline boundary condition is that, when the shoreline position is known, then the computational domain automatically contains the complete wet region where the equations of motion are applicable. However, the coordinate transformation modifies the governing equations and makes them slightly more complicated. Especially when the complete depth integrated, wave averaged equations are to be solved using this method, it requires short wave averaged flow properties e.g. radiation stresses and wave volume fluxes, to be specified along the transformed grid. Thus a wave driver is required which can provide these on the non-rectangular and time varying grid.

1.3 Outline of present work

In the next chapter, the governing equations for the nearshore circulation model SHORECIRC and it's solution method will be described. In chapter (3), a derivation of the equations for the motion of the shoreline for depth integrated, wave averaged models will be presented. This will then be used to implement a moving shoreline boundary condition for the model SHORECIRC.

Chapter (4) will describe a coordinate transformation scheme which will be used to include the effect of the moving shoreline, and which, in a general case, is also irregular in the longshore direction. As mentioned, the transformation scheme will be chosen such that it also provides a reduced grid spacing near the shoreline. It will enable the model to pick up more information near the shoreline where the hydrodynamic properties change rapidly with the cross-shore distance.

Then a fixed grid method will be described in the chapter (5). In this scheme, the shoreline position will be calculated by solving the equations for the shoreline motion, derived in chapter (3). This will provide direct information about the position of the shoreline which is treated as a special point between the last wet and the first dry grid points.

Chapter (6) will contain comparison of the results between the model computations with the shoreline boundary condition implemented using both these methods and the analytical results for one dimensional cases as given by Carrier and Greenspan (1958) and Synolakis (1987) and the numerical results for two dimensional cases given by Zelt (1986) and Özkan Haller and Kirby (1997). Finally, in chapter (7) some conclusion and the line of future work will be described.

Chapter 2

GOVERNING EQUATIONS

2.1 Governing equations

The governing equations used in the present work are the wave averaged, depth integrated Navier-Stokes equations. They were first derived by Putrevu and Svendsen (1991). Further modifications of these equations were carried out by Van-Dongeren and Svendsen (1997b), Sancho and Svendsen (1997a) and Haas and Svendsen (2000) and the final form of these equations are,

The continuity equation,

$$\frac{\partial \bar{\zeta}}{\partial t} + \frac{\partial}{\partial x_\alpha}\left(\overline{\int_{-h_0}^{\zeta} V_\alpha dz} + Q_{w\alpha}\right) = 0 \tag{2.1}$$

and the momentum equation,

$$\begin{aligned}\frac{\partial \bar{Q}_\beta}{\partial t} &+ \frac{\partial}{\partial x_\alpha}\left(\frac{\bar{Q}_\alpha \bar{Q}_\beta}{h}\right) + \frac{\partial}{\partial x_\alpha}\int_{-h_0}^{\bar{\zeta}} V_{1\alpha}V_{1\beta}dz + \frac{\partial}{\partial x_\alpha}\overline{\int_{\zeta_t}^{\zeta}\left(u_{w\alpha}V_{1\beta} + u_{w\beta}V_{1\alpha}\right)dz} \\ &+ g(h_0+\bar{\zeta})\frac{\partial \bar{\zeta}}{\partial x_\beta} - \frac{\tau_\beta^S}{\rho} + \frac{\tau_\beta^B}{\rho} + \frac{1}{\rho}\frac{\partial}{\partial x_\alpha}\left(S_{\alpha\beta} - \overline{\int_{-h_0}^{\zeta}\tau_{\alpha\beta}dz}\right) = 0\end{aligned} \tag{2.2}$$

where subscripts α and β are the indices for the horizontal co-ordinates. Figure 2.1 shows the definition of different variables used.

These equations can be rearranged so that all the terms that represent the contributions to changes in the Riemann variables along the characteristics when these equations are written in the conservation form are on the right hand side of the equations.

$$\frac{\partial \zeta}{\partial t} + \frac{\partial Q_\alpha}{\partial x_\alpha} = R_1 \tag{2.3}$$

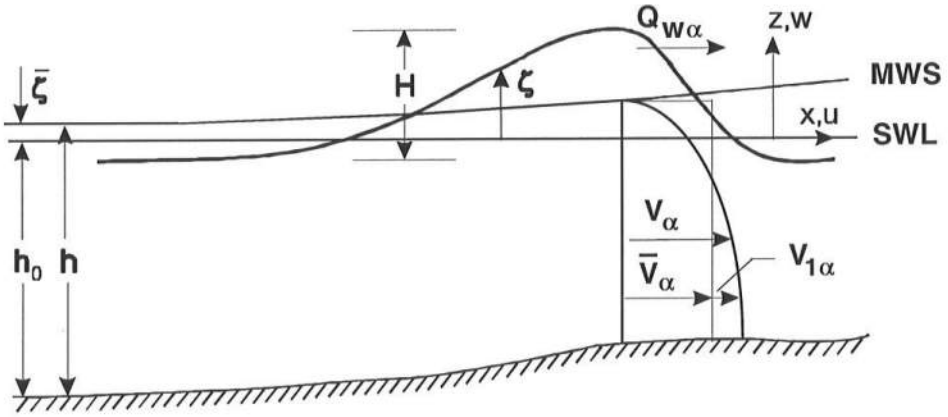

Figure 2.1: Definition sketch.

$$\frac{\partial Q_\beta}{\partial t} + \frac{\partial}{\partial x_\alpha}\left(\frac{Q_\alpha Q_\beta}{h}\right) + g(h_0+\zeta)\frac{\partial \zeta}{\partial x_\beta} = R_{2\beta} \tag{2.4}$$

Here R_1 and $R_{2\beta}$ include the short wave forcing, the dispersive mixing, the surface and bottom shear stress and the turbulent stress terms and are called the source terms. Similarly, in the case of a Boussinesq approximation these source terms contribution on the RHS may represent the dispersive-nonlinear terms.

These source terms do not change principal nature of the problem so they are disregarded for simplicity in the following numerical computations. This simplifies the governing equations which reduce to the nonlinear shallow water equations which are given by,

$$\frac{\partial \zeta}{\partial t} + \frac{\partial Q_x}{\partial x} + \frac{\partial Q_y}{\partial y} = 0 \tag{2.5}$$

$$\frac{\partial Q_x}{\partial t} + \frac{\partial}{\partial x}\left(\frac{{Q_x}^2}{h}\right) + \frac{\partial}{\partial y}\left(\frac{Q_y Q_x}{h}\right) + g(h_0+\zeta)\frac{\partial \zeta}{\partial x} = 0 \tag{2.6}$$

$$\frac{\partial Q_y}{\partial t} + \frac{\partial}{\partial x}\left(\frac{Q_x Q_y}{h}\right) + \frac{\partial}{\partial y}\left(\frac{{Q_y}^2}{h}\right) + g(h_0+\zeta)\frac{\partial \zeta}{\partial y} = 0 \tag{2.7}$$

2.2 Numerical solution scheme

A predictor-corrector method was used in the numerical scheme for time integration of the governing equations (2.5), (2.6) and (2.7). This method involves solution in two steps. One is an explicit step called predictor step which provides a first estimate of the variables at the next time step and the second is an implicit step called the corrector step which uses the values predicted by the explicit step to obtain more accurate values of the variables at that time step. More details on these time integration scheme can be found in Anderson *et al.* (1984). For example, the predictor step of an equation like,

$$\frac{\partial f}{\partial t} = F \tag{2.8}$$

will be of the form,

$$f_p{}^{n+1} = f^n + \Delta t * P(F^n, F^{n-1}, F^{n-2}, ...) \tag{2.9}$$

Whereas the form of the corrector step for this example will be,

$$f_c{}^{n+1} = f^n + \Delta t * C(F_p{}^{n+1}, F^n, F^{n-1}, F^{n-2}, ...) \tag{2.10}$$

Here superscripts show the time step at which the values are calculated and (^{n}, $^{n-1}$, $^{n-2}$ $\cdots$) are the present and the previous time steps, whereas ($^{n+1}$) is the next time step where the solution is to be obtained. The subscript ($_p$) and ($_c$) denote the predictor and the correct steps respectively. The functions P and C depend on the order of the time integration scheme used.

For high accuracy, the corrector step has to be repeated till the result converges. However, in the present work the corrector step has been executed only once as it has been found that for these set of equations and for the range of Δx and Δt used here, a second corrector step would be fairly close to the first corrector step.

The advantage of this kind of system is that, it has the simplicity of an explicit method and at the same time the results have the accuracy and the stability characteristics of an implicit method.

When all the other terms from the LHS of the governing equations (2.5), (2.6) and (2.7) except the time derivative term are moved to the RHS, these equations get the form of (2.8) and can be solved by the method described above. In the present work, a third order predictor-corrector scheme was used. In which case the functions P and C are given by,

$$P(F^n, F^{n-1}, F^{n-2}) = \frac{1}{12}\left(23F^n - 16F^{n-1} + 5F^{n-2}\right) \tag{2.11}$$

$$C(F_p^{n+1}, F^n, F^{n-1}) = \frac{1}{12}\left(5F_p^{n+1} + 8F^n - F^{n-1}\right) \tag{2.12}$$

Spatial derivatives need to be calculated before the time integration scheme, as described above, can be implemented. They were calculated by using a fourth order finite difference formula for the interior points. At the last two points near the lateral and the offshore boundaries, second order finite difference formulae were used. Forward differencing was used at the offshore and the left lateral boundaries, backward differencing was used at the right lateral boundary whereas in the interior region, central differencing was used.

At the shoreline boundary, where these sets of governing equations are not valid as the waterdepth goes to zero, the governing equations and the methods to include them in the rest of the model simulations will be described in the next chapters.

The solutions obtained were filtered using the filters described by Shapiro (1970) to get rid of the high frequency spurious solutions. This filter removes all the waves of wavelength equal to $2\Delta x$.

More details on the derivation of the governing equations and the solution scheme can be found in Putrevu and Svendsen (1994), VanDongeren and Svendsen (1997b) and VanDongeren and Svendsen (2000).

Chapter 3

MOTION OF THE SHORELINE

The depth averaged equations as described in chapter (2), give the fluid flow in terms of the volume fluxes and the surface elevation. At the shoreline, where the waterdepth goes to zero, the volume fluxes also become zero, but the velocity of the fluid particles, which are calculated by dividing the fluxes by the waterdepth, may not become zero. This velocity can't be calculated by using the depth integrated equations of motion as the waterdepth is zero there. In this chapter we will derive the equations to calculate the velocities at the shoreline and the shoreline position, once the velocities are known.

3.1 Kinematic condition

The kinematic condition at the shoreline states that the fluid particles at the shoreline remains at the shoreline. This provides us with an equation to calculate the time variation of the shoreline position when the particle velocity at the shoreline is known. If $\xi = \xi(y,t)$ is the x coordinate for the shoreline then the shoreline is given by

$$x - \xi = 0 \tag{3.1}$$

We therefore, have the kinematic condition,

$$\frac{D(x-\xi)}{Dt} = 0 \tag{3.2}$$

Where

$$\frac{D}{Dt} = \frac{\partial}{\partial t} + u^s \frac{\partial}{\partial x} + v^s \frac{\partial}{\partial y} \tag{3.3}$$

is the derivative following the shoreline. On expanding the derivatives we get,

$$\frac{\partial \xi}{\partial t} = u^s - v^s \frac{\partial \xi}{\partial y} \tag{3.4}$$

The assumption here is that the shoreline position is a single valued, continuous function of the longshore co-ordinate y at any time t.

3.2 The differential form of the momentum equation

The velocity of the shoreline can be obtained from the momentum equation by taking it's limit as the waterdepth goes to zero at the shoreline. In the following section, the differential and the integral form of the momentum equation will be used in two independent derivations of the equation for the velocity of the shoreline.

As described in chapter (2) we consider the depth integrated x momentum equation in the form,

$$\frac{\partial Q_x}{\partial t} + \frac{\partial}{\partial x}\left(\frac{{Q_x}^2}{h}\right) + \frac{\partial}{\partial y}\left(\frac{Q_x Q_y}{h}\right) + gh\frac{\partial \zeta}{\partial x} = 0 \tag{3.5}$$

where $h = h_0 + \zeta$, is the total waterdepth, $Q_x = uh$ and $Q_y = vh$ are the volume fluxes and u and v are the components of the velocity in x and y directions, respectively.

On substituting $Q_x = uh$ and $Q_y = vh$ in (3.5) we get,

$$h\frac{\partial u}{\partial t} + u\frac{\partial h}{\partial t} + u\frac{\partial Q_x}{\partial x} + uh\frac{\partial u}{\partial x} + u\frac{\partial Q_y}{\partial y} + vh\frac{\partial u}{\partial y} + gh\frac{\partial \zeta}{\partial x} = 0 \tag{3.6}$$

The continuity equation states,

$$\frac{\partial \zeta}{\partial t} + \frac{\partial Q_x}{\partial x} + \frac{\partial Q_y}{\partial y} = 0 \tag{3.7}$$

Since, $h = h_0 + \zeta$ and h_0 is a function of spatial position only, so, $\partial\zeta/\partial t = \partial h/\partial t$ and on eliminating $\partial\zeta/\partial t$ and $\partial h/\partial t$ from (3.6) and (3.7), we arrive at,

$$h\frac{\partial u}{\partial t} + hu\frac{\partial u}{\partial x} + hv\frac{\partial u}{\partial y} + gh\frac{\partial \zeta}{\partial x} = 0 \tag{3.8}$$

or, for any arbitrarily small $h \neq 0$,

$$\frac{\partial u}{\partial t} + u\frac{\partial u}{\partial x} + v\frac{\partial u}{\partial y} + g\frac{\partial \zeta}{\partial x} = 0 \tag{3.9}$$

Since the shoreline is following the fluid particles, we have

$$\frac{du^s}{dt} = \frac{\partial u}{\partial t} + \left(u\frac{\partial u}{\partial x}\right)^s + \left(v\frac{\partial u}{\partial y}\right)^s \tag{3.10}$$

On substituting from (3.10) into (3.9), we get,

$$\frac{du^s}{dt} = -g\zeta_x^s \tag{3.11}$$

Equation (3.9) is the non-trivial solution of (3.8) for any arbitrarily small waterdepth $h \neq 0$. However, at the shoreline waterdepth does go to zero. So it will be shown below that the use of integral form of the momentum equation also result in the same equation for the velocity of the shoreline before it is used in further computations.

3.3 Integral form of the momentum equation

The integral form of the x momentum equation for a control volume following fluid particles,

$$\rho\frac{d}{dt}\int_{\Omega(t)} u d\omega = -\int_{S(t)} p n_x ds \tag{3.12}$$

Here $\Omega(t)$ is the control volume of the fluid, following particle motion, contained in the control surface $S(t)$. $d\omega$ and ds are the volume and the surface elements respectively and n_x is the x component of the vector $\vec{n}$ normal to the control surface.

To simplify the calculation of the volume and the surface integrals in the equation (3.12), the region near the shoreline can be approximated by a triangular wedge as shown in the Figure 3.1. Here surface (1) moves with the free surface and it's rightmost point follows the shoreline. If we assume that u is constant within this wedge and thus is equal to the shoreline velocity u^s, then we get,

$$\rho\frac{d}{dt}\int_{\Omega(t)} u d\omega \cong \rho A\frac{du^s}{dt} \tag{3.13}$$

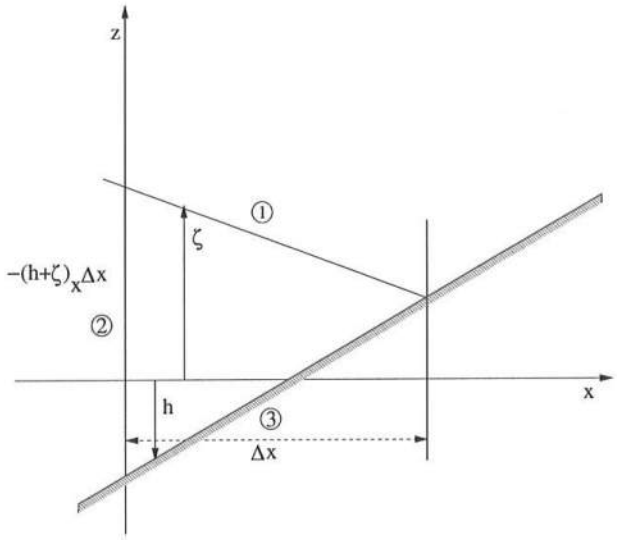

Figure 3.1: Region near the shoreline approximated by a triangular wedge.

where, $A = -\frac{1}{2}(h+\zeta)_x \Delta x^2$ is the cross section area of the wedge. Since x is positive in the onshore direction and the waterdepth is positive offshore for $(h+\zeta)_x < 0$, A has a negative sign in the expression here.

If we assume the pressure to be hydrostatic near the shoreline, we get

$$\begin{aligned} -\int_S \frac{p}{\rho} n_x ds &= \frac{1}{2} g \left[(h+\zeta)_x \Delta x\right]^2 \\ &\quad -\frac{1}{2} g (h+\zeta)_x \Delta x \frac{h_x}{\sqrt{1+h_x^2}} \left(\Delta x \sqrt{1+h_x^2}\right) \qquad (3.14) \\ &= \frac{1}{2} g \Delta x^2 \zeta_x (h+\zeta)_x \qquad (3.15) \end{aligned}$$

On substituting the terms on the LHS of (3.13) and (3.15) into (3.12), we get,

$$\frac{du^s}{dt} = -g\zeta_x^s \qquad (3.16)$$

This is the same equation as (3.11) obtained in the section (3.2).

On extending this to the 2DH case, x and y components of the velocity of the shoreline can be given by,

$$\left.\frac{du^s(y,t)}{dt}\right|_y = -g\zeta_x^s \tag{3.17}$$

and,

$$\left.\frac{dv^s(y,t)}{dt}\right|_y = -g\zeta_y^s \tag{3.18}$$

Here u^s and v^s are calculated along a constant y line so that the shoreline motion can be calculated by (3.4). Hence equations (3.17) and (3.18) represent the general 2DH equations which will be used in the following to determine the horizontal velocities of the shoreline points with co-ordinates (x^s, y^s).

3.4 Discussion

As mentioned in the introduction, the question that remains to be answered now is, how to incorporate a time varying domain in a numerical scheme. This can be achieved in two ways.

The first is to map the physical domain onto a new co-ordinate system which follows the time varying domain and perform all the calculations in the transformed domain. This transformation not only modifies the governing equations but also gives us an opportunity to obtain a spatial distribution of grid spacing so that a higher resolution can be obtained in the areas where the gradients of the surface elevation and the velocities are expected to be higher. This approach and a scheme to implement this in SHORECIRC model will be discussed in detail in chapter (4).

The second method could be, to have a fixed grid and define the shoreline position as an interface between wet and dry grid points. In this method the governing equations remain unmodified, though new finite difference formulations need to be obtained to take into account a non-constant grid spacing between the last wet grid point and the shoreline position. An algorithm also needs to be formulated to add and delete grid points from the active calculation zone, which is the wet region

of the computational domain, as the grid points get wet and dry in the course of a model run. We describe a scheme to implement this method of treatment of the moving shoreline for SHORECIRC in chapter (5).

Chapter 4

THE COORDINATE TRANSFORMATION SCHEME

One of the methods of implementation of a time varying domain in a numerical model is to introduce a coordinate transformation such that the instantaneous physical domain, which expands and contracts as the shoreline is moving, gets mapped on to a fixed domain in the transformed coordinate system. One such scheme will be described here. Near the shoreline, velocities and surface elevations often have large gradients. A suitable coordinate transformation can be chosen such that such a smaller grid spacing can be obtained as an add-on benefit in the regions where high resolution is required. So a high resolution near the shoreline than the rest of the domain will produce a more accurate result at a lesser computational cost. In selecting a coordinate transformation scheme, which has a primary aim of mapping the irregular and time varying shoreline onto a fixed grid in the computational domain, constraints will be prescribed here so that a smaller grid spacing near the shoreline than the rest of the domain can be obtained. This transformation is expected to result in a computational grid, which has evenly spaced grid points in the computational domain, and which corresponds to a grid with varying spacing in the physical domain at any given time.

The governing equations described in the chapter (2) are derived for rectangular cartesian coordinates. On introduction of this coordinate transformation, the governing equations need to be modified to take into account the grid spacing variation and distortion. An example of a such modification of the governing equation

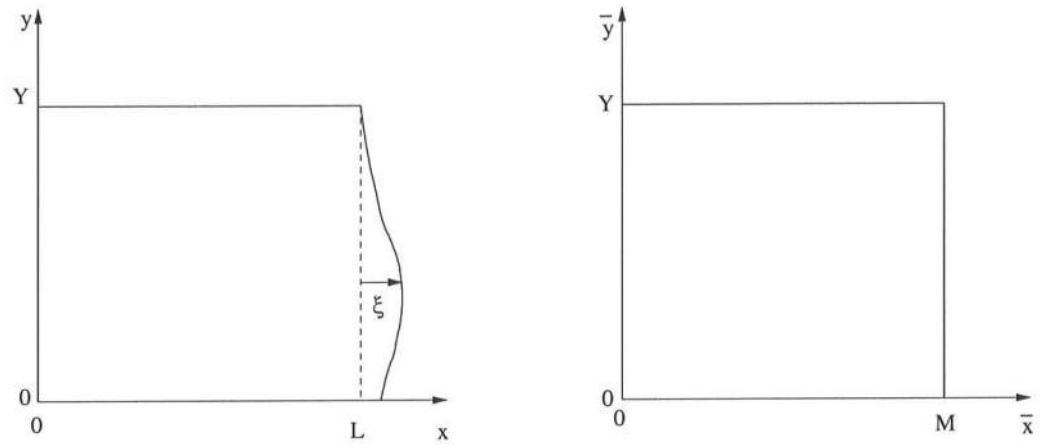

Figure 4.1: Sketches of the real (on the left) and the transformed (on the right) model domains.

due to introduction of a coordinate transformation is described by Anderson *et al.* (1984) to take into account a non-uniform grid spacing in a model domain.

4.1 Model domain definitions

The actual physical domain (x, y, t) extends from $x = 0$ to $x = L + \xi$ and $y = 0$ to $y = Y$. $\xi(y, t)$ is the shoreline position measured from a reference level $x = L$. In most cases the initial shoreline position can be taken to be this reference level. The physical domain is transformed onto a computational domain $(\bar{x}, \bar{y}, \bar{t})$ by the transformation equations,

$$x = g(\bar{x}) + \xi(y, t) f(\bar{x}) \tag{4.1}$$

$$y = \bar{y} \tag{4.2}$$

$$t = \bar{t} \tag{4.3}$$

The computational domain extends from $\bar{x} = 0$ to $\bar{x} = M$ and $\bar{y} = 0$ to $\bar{y} = Y$. A sketch of the real and the computational domains are shown in the Figure 4.1.

4.2 Conditions on the transformation functions

The form of the transformation equation (4.1) is selected to suit the goal of the transformation. The function $f(\bar{x})$ is selected such that the transformation maps the irregular shoreline onto a fixed, straight line in the computational domain whereas the function $g(\bar{x})$ is selected such that this transformation yields smaller grid spacing near the shoreline than that offshore.

Since the offshore boundary of the real and the computational domains should be at the same location,

$$\bar{x} = 0 \quad \Rightarrow \quad x = 0 \tag{4.4}$$

we must have,

$$f(0) = 0 \quad ; \quad g(0) = 0 \tag{4.5}$$

Similarly the shoreline in both the domains must coincide, so,

$$\bar{x} = M \quad \Rightarrow \quad x = L + \xi \tag{4.6}$$

Hence, f and g must satisfy,

$$f(M) = 1 \quad ; \quad g(M) = L \tag{4.7}$$

Additionally, $f(\bar{x}) \to 0$ as $\bar{x}$ tends to zero, so that the effect of the shoreline changes reduces offshore gradually and finally vanishes at the offshore boundary of the computational domain.

Without loss of generality, we can assume that $L = M$ as it does simplify the calculations later on. Now $\Delta x/\Delta\bar{x} = 1$ implies an equal grid spacing in both the domains.

The grid size distribution in the cross-shore direction is given by,

$$\frac{\Delta x}{\Delta \bar{x}} = g'(\bar{x}) + \xi(y,t) f'(\bar{x}) \tag{4.8}$$

The condition that the grid spacing near the shoreline should be smaller than that offshore, is expressed mathematically by,

$$0 < \left[\left(\frac{\Delta x}{\Delta \bar{x}} \right)_{\bar{x}=M} = g'(M) + \xi(y,t) f'(M) \right] < 1 \tag{4.9}$$

$\Delta x / \Delta \bar{x} = 0$ would imply that two points in the computational domain correspond to one point in the physical domain. Since the inverse of the transform would not be unique in this case, it must be avoided in the transformation used here.

4.3 Selection of the transformation functions

Any function which satisfies the conditions described in the section (4.2) can be used in the transformation equations. The conditions on the function $f(\bar{x})$ state that it goes from 1 to 0 as $\bar{x}$ goes from the shoreline $\bar{x} = M$ to the offshore boundary of the model domain $\bar{x} = 0$.

Different analytical functions which have a variation with $\bar{x}$ similar to the one required by the conditions on $f(\bar{x})$ were tried. Figure (4.2) shows the variation of some of them. e.g.

$$f_1(\bar{x}) = e^{-\alpha(M-\bar{x})} \tag{4.10}$$

$$f_2(\bar{x}) = e^{-\alpha(M-\bar{x})^2} \tag{4.11}$$

$$f_3(\bar{x}) = 1 - \tanh\{\alpha(M-\bar{x})\} \tag{4.12}$$

$$f_4(\bar{x}) = \left(\frac{\bar{x}}{M} \right) e^{-\alpha(M-\bar{x})} \tag{4.13}$$

and,

$$f_5(\bar{x}) = (e^{-\alpha(M-\bar{x})} - e^{-\alpha M})/(1 - e^{-\alpha M}). \tag{4.14}$$

The last two functions satisfy condition $f(0) = 0$ exactly, whereas, the other three can give $f(\bar{x})$ very close to zero depending on the values of α and M but never equal to zero at the offshore boundary.

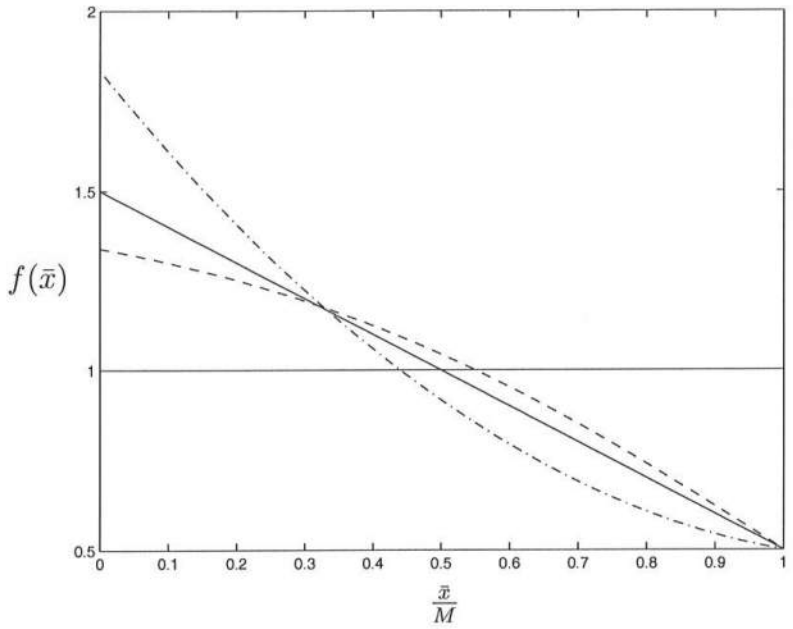

Figure 4.2: Some possible choices for $f(\bar{x})$. (———) $e^{-\alpha(M-\bar{x})}$; (– – –) $e^{-\alpha(M-\bar{x})^2}$; (–·–·–) $1 - \tanh\{\alpha(M - \bar{x})\}$; (· · ·) $\left(\frac{\bar{x}}{M}\right) e^{-\alpha(M-\bar{x})}$ and (·····) $(e^{-\alpha(M-\bar{x})} - e^{-\alpha M})/(1 - e^{-\alpha M})$ for $\alpha = 0.3$.

Since the purpose of the function $g(\bar{x})$ is to ensure a certain variation of $\Delta x/\Delta\bar{x}$ which is related to $g'(\bar{x})$, it is convenient to prescribe $g'(\bar{x})$, subject to,

$$g'(M) < 1 \tag{4.15}$$

and,

$$\int_0^M g'(\omega)d\omega = M \tag{4.16}$$

and then calculate $g(\bar{x})$ by,

$$g(\bar{x}) = \int_0^{\bar{x}} g'(\omega)d\omega \tag{4.17}$$

For any $f'(M) \neq 0$, the grid size distribution $\Delta x/\Delta\bar{x}$ will be greater or smaller there than $g'(M)$ depending on the sign of ξ. If $g'(M) = 0.5$, then for any given $f'(M)$, $(\Delta x/\Delta\bar{x})_{\bar{x}=M}$ can accommodate maximum variation of ξ about $\xi = 0$. In most of the simulations described afterward, $g'(M) = 0.5$ will be used. Figure 4.3 shows the effect of different ξ on $\Delta x/\Delta\bar{x}$ for one particular choice of $f(\bar{x})$ and $g(\bar{x})$. It can be seen, that the grid spacing near the shoreline ($\bar{x} = M$) is smaller than

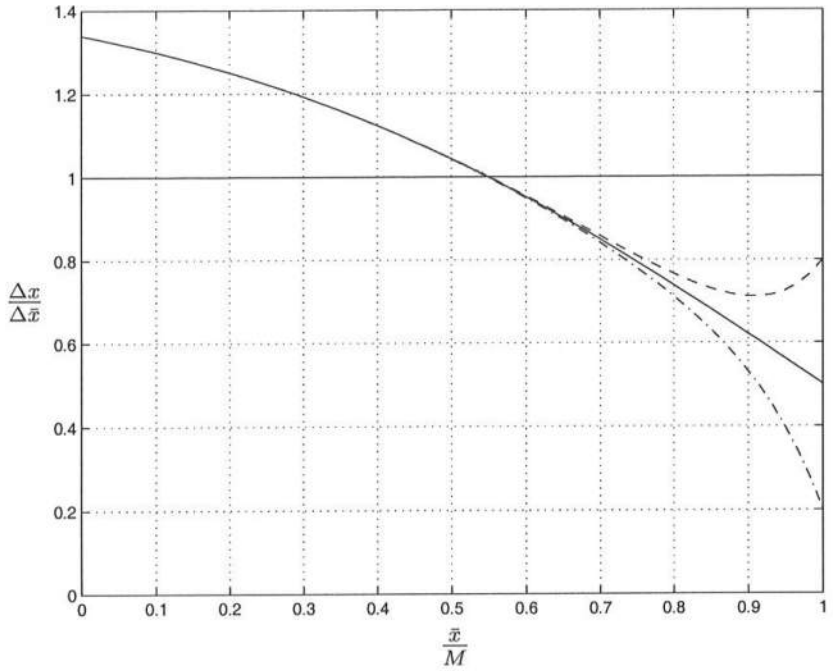

Figure 4.3: $\Delta x/\Delta\bar{x}$ for different ξ with $f(\bar{x}) = f_5(\bar{x})$ and $g'(\bar{x}) = 0.5+\tanh\{a(M-\bar{x})\}$. (———) $\xi = 0$; (– – –) $\xi = 3$; (–·–·–) $\xi = -3.0$, for $a = .01015$ and $\alpha = 0.1$.

that offshore ($\bar{x} = 0$) but it changes with ξ. During the highest run-up ($\xi = 3$ in the example) the grid is stretched and $\Delta x/\Delta\bar{x}$ increases somewhat toward the shoreline. When the shoreline is in the lowest position of rundown ($\xi = -3$) the resolution at the shoreline is very high with $\Delta x/\Delta\bar{x} = 0.2$ only. Thus a very high resolution is obtained during phase of the rundown which is also the phase with the strongest spatial variations and potential wave breaking.

As there are only two required conditions on the function $g(\bar{x})$ and one of them has been used to determine the value of $g'(M)$ only one condition is left on $g(\bar{x})$. It can be uniquely determined if it has only one free parameter. If for example a polynomial of $\bar{x}$ is assumed for $g'(\bar{x})$, only a linear function can be determined uniquely and that is,

$$g'(\bar{x}) = 0.5 + \frac{M - \bar{x}}{M} \tag{4.18}$$

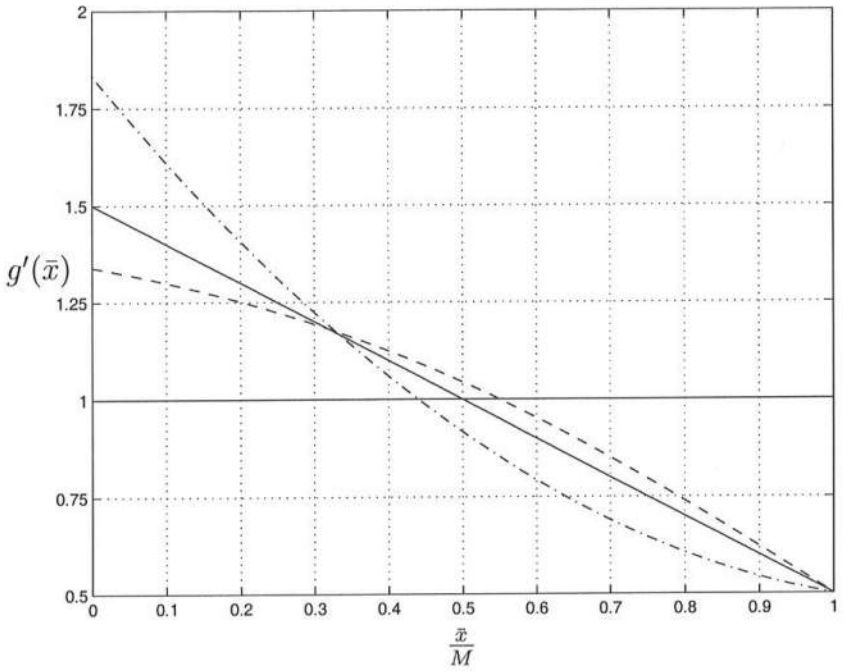

Figure 4.4: Some possible choices for $g'(\bar{x})$. (———) $0.5 + (M - \bar{x})/M$; (– – –) $0.5 + \tanh\{a(M - \bar{x})\}$ and (–·–·–) $0.5 + a\,(M - \bar{x}) + b\,(M - \bar{x})^2$ with $a = 1/3M$ and $b = 1/M^2$ for $M = 20m$.

For a second degree polynomial, a family of functions for $g'(\bar{x})$ given by,

$$g'(\bar{x}) = 0.5 + a\,(M - \bar{x}) + b\,(M - \bar{x})^2 \tag{4.19}$$

is obtained. Where a and b must satisfy the relation,

$$3aM + 2bM^2 = 3 \tag{4.20}$$

which is obtained by substituting (4.19) into the condition (4.16)

Different functions have been tested for $g(\bar{x})$ too. Figure 4.4 shows some possible choices for $g(\bar{x})$. For the most of the model simulations described afterward $g'(\bar{x}) = 0.5 + \tanh\{a(M - \bar{x})\}$. Here a is calculated so that $g(0) = 0$ is satisfied. It can be seen in Figure 4.4 that the region where $g'(\bar{x}) < 1$ is smaller for $g'(\bar{x}) = 0.5 + \tanh\{a(M - \bar{x})\}$. So the region of $\Delta x/\Delta\bar{x} < 1$ is concentrated near the shoreline where a high resolution is required. $f(\bar{x}) = f_5(\bar{x})$ from (4.14) has been used in the

most of the simulations. $f(\bar{x})$ satisfies all the conditions prescribed for any value of α, which is however, selected such that $e^{-\alpha M}$ is very small and close to zero.

4.4 Modification of the governing equations due to the transformation

In order to be able to perform calculations in the $(\bar{x}, \bar{y}, \bar{t})$ coordinate system, the derivatives with respect to x, y and t in the continuity and the momentum equations need to be changed to the derivatives with respect to $\bar{x}$, $\bar{y}$ and $\bar{t}$. These changes can be obtained by successive differentiation. For the general case of $x = f(\bar{x}, \bar{y}, \bar{t})$, $y = f(\bar{x}, \bar{y}, \bar{t})$ and $t = f(\bar{x}, \bar{y}, \bar{t})$ the modified differential operators would be,

$$\frac{\partial}{\partial x} = \frac{\partial}{\partial \bar{x}}\frac{\partial \bar{x}}{\partial x} + \frac{\partial}{\partial \bar{y}}\frac{\partial \bar{y}}{\partial x} + \frac{\partial}{\partial \bar{t}}\frac{\partial \bar{t}}{\partial x} \tag{4.21}$$

$$\frac{\partial}{\partial y} = \frac{\partial}{\partial \bar{x}}\frac{\partial \bar{x}}{\partial y} + \frac{\partial}{\partial \bar{y}}\frac{\partial \bar{y}}{\partial y} + \frac{\partial}{\partial \bar{t}}\frac{\partial \bar{t}}{\partial y} \tag{4.22}$$

$$\frac{\partial}{\partial t} = \frac{\partial}{\partial \bar{x}}\frac{\partial \bar{x}}{\partial t} + \frac{\partial}{\partial \bar{y}}\frac{\partial \bar{y}}{\partial t} + \frac{\partial}{\partial \bar{t}}\frac{\partial \bar{t}}{\partial t} \tag{4.23}$$

However in the present formulation, $\bar{x}$ is a function of x, y and t whereas $\bar{y}$ and $\bar{t}$ are functions of only y and t, respectively, so,

$$\frac{\partial \bar{y}}{\partial x} = \frac{\partial \bar{y}}{\partial t} = 0 \tag{4.24}$$

$$\frac{\partial \bar{t}}{\partial x} = \frac{\partial \bar{t}}{\partial y} = 0 \tag{4.25}$$

Furthermore from (4.2) and (4.3),

$$\frac{\partial \bar{y}}{\partial y} = \frac{\partial \bar{t}}{\partial t} = 1 \tag{4.26}$$

With these simplifications, (4.21), (4.22) and (4.23) reduce to,

$$\frac{\partial}{\partial x} = \frac{\partial}{\partial \bar{x}}\frac{\partial \bar{x}}{\partial x} \tag{4.27}$$

$$\frac{\partial}{\partial y} = \frac{\partial}{\partial \bar{y}} + \frac{\partial}{\partial \bar{x}}\frac{\partial \bar{x}}{\partial y} \tag{4.28}$$

$$\frac{\partial}{\partial t} = \frac{\partial}{\partial \bar{t}} + \frac{\partial}{\partial \bar{x}}\frac{\partial \bar{x}}{\partial t} \tag{4.29}$$

Differentiating the transformation equation (4.1) with respect to x, y and t gives,

$$1 = g'(\bar{x})\frac{\partial \bar{x}}{\partial x} + \xi(y,t)f'(\bar{x})\frac{\partial \bar{x}}{\partial x} \tag{4.30}$$

$$0 = g'(\bar{x})\frac{\partial \bar{x}}{\partial y} + \xi(y,t)f'(\bar{x})\frac{\partial \bar{x}}{\partial y} + \frac{\partial \xi(y,t)}{\partial y}f(\bar{x}) \tag{4.31}$$

and,

$$0 = g'(\bar{x})\frac{\partial \bar{x}}{\partial t} + \xi(y,t)f'(\bar{x})\frac{\partial \bar{x}}{\partial t} + \frac{\partial \xi(y,t)}{\partial t}f(\bar{x}) \tag{4.32}$$

respectively. By rearranging (4.30), (4.31) and (4.32) we get,

$$\frac{\partial \bar{x}}{\partial x} = \frac{1}{g'(\bar{x}) + \xi(y,t)f'(\bar{x})} \tag{4.33}$$

$$\frac{\partial \bar{x}}{\partial y} = -\left\{\frac{1}{g'(\bar{x}) + \xi(y,t)f'(\bar{x})}\right\}\frac{\partial \xi(y,t)}{\partial y}f(\bar{x}) \tag{4.34}$$

$$\frac{\partial \bar{x}}{\partial t} = -\left\{\frac{1}{g'(\bar{x}) + \xi(y,t)f'(\bar{x})}\right\}\frac{\partial \xi(y,t)}{\partial t}f(\bar{x}) \tag{4.35}$$

Or,

$$\frac{\partial \bar{x}}{\partial y} = -\frac{\partial \bar{x}}{\partial x}\frac{\partial \xi}{\partial y}f(\bar{x}) \tag{4.36}$$

$$\frac{\partial \bar{x}}{\partial t} = -\frac{\partial \bar{x}}{\partial x}\frac{\partial \xi}{\partial t}f(\bar{x}) \tag{4.37}$$

Substitution from (4.27), (4.36) and (4.37) in equations (4.28) and (4.29) results in,

$$\frac{\partial}{\partial y} = \frac{\partial}{\partial \bar{y}} - \frac{\partial}{\partial \bar{x}}\frac{\partial \bar{x}}{\partial x}\frac{\partial \xi}{\partial y}f(\bar{x}) \tag{4.38}$$

$$\frac{\partial}{\partial t} = \frac{\partial}{\partial \bar{t}} - \frac{\partial}{\partial \bar{x}}\frac{\partial \bar{x}}{\partial x}\frac{\partial \xi}{\partial t}f(\bar{x}) \tag{4.39}$$

On applying these modifications from (4.27), (4.38) and (4.39) to (2.5), (2.6) and (2.7), we obtain the governing equations in their final form as,

$$\frac{\partial \zeta}{\partial \bar{t}} - \frac{\partial \zeta}{\partial \bar{x}}\frac{\partial \bar{x}}{\partial x}\frac{\partial \xi}{\partial t}f(\bar{x}) + \frac{\partial Q_x}{\partial \bar{x}}\frac{\partial \bar{x}}{\partial x} + \frac{\partial Q_y}{\partial \bar{y}} - \frac{\partial Q_y}{\partial \bar{x}}\frac{\partial \bar{x}}{\partial x}\frac{\partial \xi}{\partial y}f(\bar{x}) = 0 \tag{4.40}$$

$$\frac{\partial Q_x}{\partial \bar{t}} - \frac{\partial Q_x}{\partial \bar{x}}\frac{\partial \bar{x}}{\partial x}\frac{\partial \xi}{\partial t}f(\bar{x}) + \frac{\partial}{\partial \bar{x}}\left(\frac{{Q_x}^2}{h}\right)\frac{\partial \bar{x}}{\partial x} + \frac{\partial}{\partial \bar{y}}\left(\frac{Q_x Q_y}{h}\right) - \frac{\partial}{\partial \bar{x}}\left(\frac{Q_x Q_y}{h}\right)\frac{\partial \bar{x}}{\partial x}\frac{\partial \xi}{\partial y}f(\bar{x}) = -gh\frac{\partial \zeta}{\partial \bar{x}}\frac{\partial \bar{x}}{\partial x} \tag{4.41}$$

$$\frac{\partial Q_y}{\partial \bar{t}} - \frac{\partial Q_y}{\partial \bar{x}}\frac{\partial \bar{x}}{\partial x}\frac{\partial \xi}{\partial t}f(\bar{x}) + \frac{\partial}{\partial \bar{x}}\left(\frac{Q_x Q_y}{h}\right)\frac{\partial \bar{x}}{\partial x} + \frac{\partial}{\partial \bar{y}}\left(\frac{{Q_x}^2}{h}\right) - \frac{\partial}{\partial \bar{x}}\left(\frac{{Q_x}^2}{h}\right)\frac{\partial \bar{x}}{\partial x}\frac{\partial \xi}{\partial y}f(\bar{x}) = -gh\left[\frac{\partial \zeta}{\partial \bar{y}} - \frac{\partial \zeta}{\partial \bar{x}}\frac{\partial \bar{x}}{\partial x}\frac{\partial \xi}{\partial y}f(\bar{x})\right] \tag{4.42}$$

When the functions $f(\bar{x})$ and $g(\bar{x})$ are selected, the term $\partial\bar{x}/\partial x$ can be calculated by (4.33). Since ξ is known as a function of y at any time step n and at the previous time steps $n-1$, $n-2$ etc. , $\partial\xi/\partial y$ can easily be calculated at those time steps. As the components of the velocity of the shoreline are also known at that present time step n and previous time steps, $\partial\xi/\partial t$ can be calculated from (3.4) and then ξ at the next time step $n+1$ can be obtained by the time integration of this equation. As all the terms in the modified governing equations (4.40), (4.41) and (4.42) are known at a time step n and previous time steps, a 3rd order ABM predictor-corrector scheme can be applied to calculate the volume fluxes and the surface elevation at the next time step for $\bar{x} = 0$ to $\bar{x} < M$. At $\bar{x} = M$ a similar predictor-corrector scheme can also be used for (3.17) and (3.18) to obtain u^s and v^s and then (3.4) to obtain shoreline position ξ at the next time step.

Chapter 5

FIXED GRIDS WITH WET-DRY INTERFACE

As mentioned earlier, the particle velocity at the shoreline and thus the shoreline position can be calculated by the equations derived in chapter (3). In the last chapter, a coordinate transformation method was described to take into account a time varying fluid domain in a numerical model. In this chapter another method of implementation of the boundary condition at the moving shoreline will be described which uses fixed grids. In this method the computational domain discretized on a fixed grid and the shoreline is defined as the point separating wet and dry regions, which need not be a grid point. In order to do this, the last wet and the first dry grid points are identified and the shoreline point is treated as a special point between the grid points. When the shoreline passes a dry grid point while moving in the shoreward direction, that grid point is included in the active calculation zone, which is the wet region of the domain, at the following time steps of the computation. Similarly when a wet grid point is passed in the seaward motion of the shoreline, it is excluded from the active calculations in the following time steps.

In the past, most of the implementations using fixed grid points with wet-dry interface, do not resolve the shoreline position between the last wet and the first dry point. Many such examples were discussed in section (1.1). Sielecki and Wurtele (1970) and VanDongeren and Svendsen (1997b) give a few examples where the shoreline position between the last wet and the first dry grid points was determined, though they use extrapolation schemes to do this. In the method used by

VanDongeren and Svendsen (1997b) the shoreline position between the last wet and the first dry point was determined along with the surface elevation at the last wet point. This was done by calculating the volume of water stored past the last wet point and assuming a linear variation of the surface elevation from the last wet point to the shoreline point. The volume flux at the last wet point was also obtained by interpolation.

In the method described here, the velocity of the fluid particles at the shoreline are obtained first. The shoreline position is then calculated by using these velocities. The actual shoreline position is calculated at each time step and thus the position of the shoreline between the last wet and the first dry grid points is known.

5.1 Spatial derivatives near the shoreline

Since the distance between the last wet point and the shoreline point is not the same as the constant grid spacing in the rest of the domain and this spacing also changes with time, the finite difference formulation for spatial derivatives near the shoreline needs to be modified. This is done by going back to the Taylor series expansion and obtaining the spatial derivative formula for a non constant grid spacing near the shoreline.

For simplicity, in the following sections only the 1DH case will be discussed. The procedure for 2DH case will be described later in the section 5.3 as a modification of 1DH case.

The shoreline position is identified as x_s, the last wet grid position as x_0 and the second last wet grid position as x_1. The spacing between x_1 and x_0 is Δx which is the grid spacing in the rest of the domain. The spacing between x_0 and x_s changes with time. The ratio of this distance to the constant grid spacing in the rest of the domain Δx is denoted by s. A sketch of the domain near the shoreline is given in Figure 5.1.

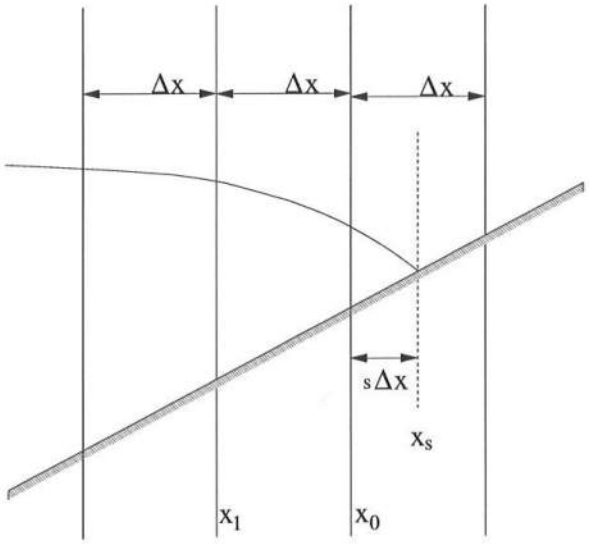

Figure 5.1: Domain near the shoreline. x_s is the shoreline position. x_0 and x_1 are last two wet points.

Let's assume that the derivatives of the function $f(x)$ are to be calculated. The Taylor series expansion of this function about the last wet grid point x_0 gives,

$$f(x_s) = f(x_0 + s\Delta x) = f(x_0) + s\Delta x f'(x_0) + \frac{(s\Delta x)^2}{2!} f''(x_0) + O(\Delta x^3) \quad (5.1)$$

$$f(x_1) = f(x_0 - \Delta x) = f(x_0) - \Delta x f'(x_0) + \frac{(\Delta x)^2}{2!} f''(x_0) + O(\Delta x^3) \quad (5.2)$$

By eliminating $f''(x_0)$ from equations (5.1) and (5.2) the relation for $f'(x_0)$ in terms of $f(x_0)$, $f(x_1)$ and $f(x_s)$ are obtained as,

$$f'(x_0) = \frac{f(x_s) + (s^2 - 1)f(x_0) - s^2 f(x_1)}{s(s+1)\Delta x} \quad (5.3)$$

Similarly, the Taylor series expansion of $f(x)$ about the shoreline position x_s gives,

$$f(x_0) = f(x_s - s\Delta x) = f(x_s) - s\Delta x f'(x_s) + \frac{(s\Delta x)^2}{2!} f''(x_s) + O(\Delta x^3) \quad (5.4)$$

$$f(x_1) = f(x_s - (s+1)\Delta x) = f(x_s) - (s+1)\Delta x f'(x_s) + \frac{((s+1)\Delta x)^2}{2!} f''(x_s) + O(\Delta x^3) \quad (5.5)$$

and elimination of $f''(x_s)$ gives,

$$f'(x_s) = \frac{(1+2s)f(x_s) - (1+s)^2 f(x_0) + s^2 f(x_1)}{s(s+1)\Delta x} \tag{5.6}$$

5.2 Addition and deletion of a grid point

In this method with a fixed grid and a wet-dry interface for the shoreline, the active calculation zone is the wet region where the fluxes and the surface elevations are calculated by solving the continuity and the momentum equations (2.5), (2.6) and (2.7). The second part of the computational domain is the dry region shoreward of x_s. This region is sufficiently described by,

$$h_0 + \zeta = 0 \tag{5.7}$$

or,

$$\zeta = -h_0 \tag{5.8}$$

where h_0 may be < 0 and,

$$Q_x = 0 \tag{5.9}$$

$$Q_y = 0 \tag{5.10}$$

At the shoreline, the velocity component is calculated using (3.17) and then the horizontal position of the shoreline point is calculated by time integration of (3.4). The surface elevation at the shoreline point is then calculated by

$$\zeta_s = -(h_0)_s \tag{5.11}$$

and the fluxes there are zero.

In the cases where the bottom topography is given analytically, h_{0s} can be calculated directly when the shoreline position is known. In other cases, it has to be obtained by interpolation between the undisturbed water depths at the regularly spaced grid points near the shoreline.

The ratio of the distance of the shoreline position from the last wet grid to the constant grid spacing Δx, s, appears in the denominator of the equations (5.3) and (5.6), so $s = 0$ must be avoided during the motion of the shoreline. Therefore, it is necessary to choose a small, fixed minimum value for $s = s_{min}$. During rundown, if $s < s_{min}$, it is assumed that the last wet grid point (x_0) has become dry, so that grid point is removed from the active calculation zone and the value of s is increased by 1.

Similarly, during run up the first dry grid point is not included in the active calculation region until the value of s becomes larger than $1 + s_{min}$. When $s > 1 + s_{min}$, the first dry grid point is declared to become a wet point and is include in the active calculation zone. The value of s is then decreased by 1. In most of the simulations described later on, we will use $s_{min} = 0.5$.

Since a third order ABM predictor-corrector method is used for time integration in this work, it's required to know the RHS of the governing equations at time steps n, $n-1$, and $n-2$ in order to calculate the flow variables at the next time step $n+1$. Therefore when a dry point is included in the active calculation region during the onshore movement of the shoreline, the RHS of the governing equations at two previous time steps is required to be specified at that grid location. However, the first dry grid point is not added to the calculation zone until after the value of s becomes greater than $1 + s_{min}$ and in the most cases, the number of time steps needed for s to go from $s = 1$ to $s = 1 + s_{min}$ is more than two. Hence at the first dry grid point, the calculation of the RHS of the mass and the momentum equations can be started as soon as the shoreline passes that point while moving in the onshore direction. This provides the values of the variables at the new wet points which can then be used in the time stepping of ζ, Q_x and Q_y when that point is included in the active calculation region. However, if the value of s_min selected is very small, the number of time steps needed for s to go from $s = 1$ to $s = 1 + s_{min}$ can become

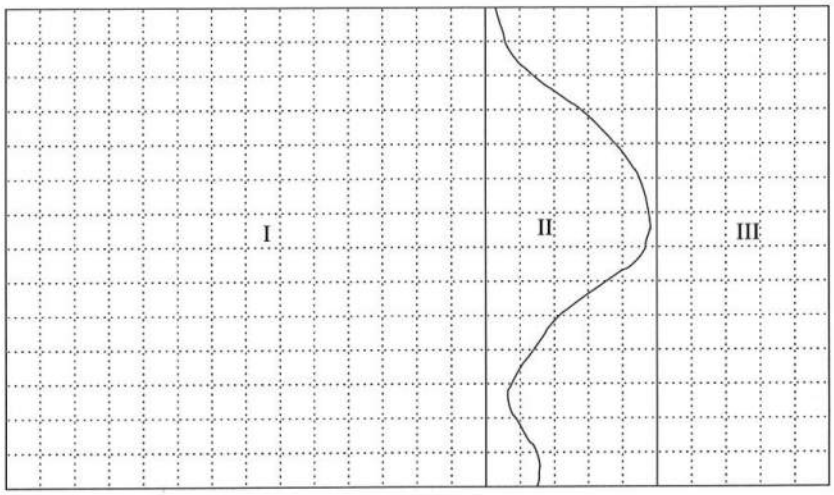

Figure 5.2: Three regions in 2DH case with fixed grid and wet-dry interface. Region I has all the grid points wet, region III has all the grid points dry and region II has some grid points which are wet.

less than two and small errors may introduce due to incorrectly imposing the RHS of the mass and the momentum equations to zero.

Shapiro filter is applied to all the wet points in the cross-shore direction. As the distance between the shoreline position and the last wet point is not constant and is not the same as the rest of the domain, the shoreline point is excluded from the filter scheme.

5.3 Fixed grids for 2DH cases

In the 2DH case, some extra care is needed in order to apply the boundary condition at the shoreline using a fixed grid and a wet-dry interface. The difference from the 1DH case is that now the last wet points and the shoreline points are functions of longshore position. The y component of the velocity is also need to be calculated using (3.18) before (3.4) can be used for calculation of the shoreline position. Thus the y derivatives are to be calculated at and near the shoreline and filters are to applied in the longshore direction y also. The difficulty in the calculation of y gradients at the shoreline is due to the fact that at an arbitrary

shoreline position, there may not be grid points in the longshore direction, as $s(y)$, in general, can have different values at different longshore locations. It can be seen in Figure 5.3 that in order to calculate derivatives at a shoreline point A, the variables at the points B and C should be known. However, as B and C are neither a regular grid point nor a shoreline point, the values of the variables at these points can only be obtained by interpolation.

As described by Shapiro (1970), filtering in 2DH cases are to be done by applying the filter first in one direction and then in the other direction. In the cross-shore direction, as the last wet point is known and all the points offshore of the last wet point are wet, the filter can be applied easily. Whereas in the longshore direction, it's necessary to find out first which grid points are wet before a filter can be applied. Depending on the number of wet points in the longshore direction, the order of filter in that direction also needs to be changed.

In an attempt to solve this problem, the model domain is divided into three regions. In the first region, all the grid points in the longshore direction are wet. In the second region some of the grid points in the longshore direction are wet, and in the third region none of the grid points in the longshore direction are wet. Figure (5.2) shows these three regions for a typical model domain. Extending the 1DH formulation to 2DH is straightforward in the regions one and three, since all the grid are either wet or dry,. In the region II, the x derivatives near the shoreline can be calculated by (5.3) and (5.6) as before. To obtain the y derivatives in this region, a fourth order central difference formula has been applied if there are two wet points on both sides of a wet point along the y direction, otherwise a second order finite difference formula has been applied.

As mentioned Figure 5.3 shows a typical case near the shoreline. In order to solve the equation (3.18) for the y component of the velocity at the shoreline point A, $\partial\zeta/\partial y$ needs to be calculated at that point. Since on the one side of

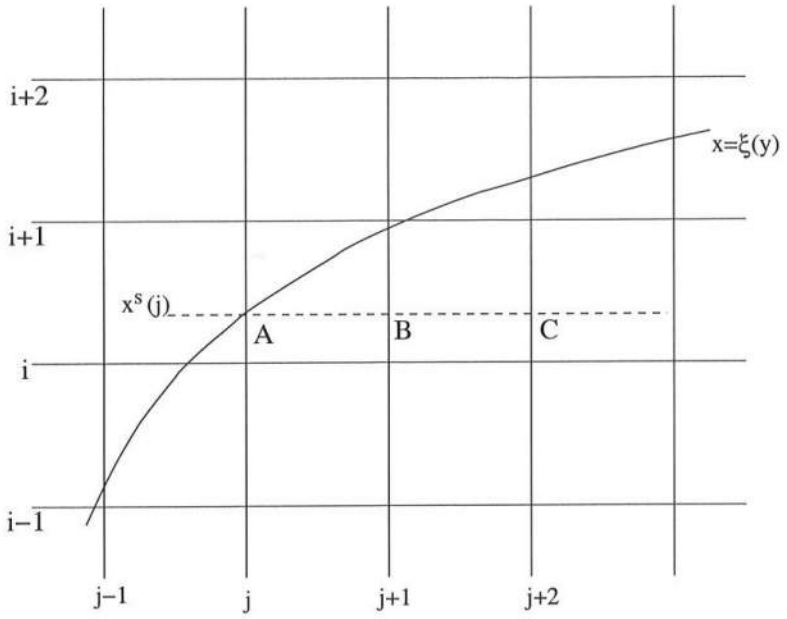

Figure 5.3: A typical situation encountered in order to calculate the y derivative at the shoreline. $(- - -)$ is the shoreline position at the j^{th} grid in the y direction.

the shoreline point A there are no grid points in the longshore direction, a second order interpolation scheme is first applied to obtain the surface elevation data in the longshore direction at points B and C in Figure 5.3 before this derivative can be calculated.

The equation,

$$f(B) = a * \{s(j)\}^2 + b * s(j) + c \tag{5.12}$$

with $s(j) = (x^s(j) - x(i))/\Delta x$, was used to calculate the value of f at point B. Here,

$$a = \frac{1}{2}\{f(i, j+1) - 2f(i-1, j+1) + f(i-2, j+1)\} \tag{5.13}$$

$$b = \frac{1}{2}\{3f(i, j+1) - 4f(i-1, j+1) + f(i-2, j+1)\} \tag{5.14}$$

and

$$c = f(i, j+1) \tag{5.15}$$

Similarly $j+1$ was replaced by $j+2$ to calculate the variables at the point C. The 2nd order forward difference equation,

$$\frac{\partial f}{\partial y}\Big|_A = \frac{1}{2\Delta y}\{-3f(A) + 4f(B) - f(C)\} \tag{5.16}$$

was then used to calculate the derivative at the point A as the distances between A and B, and B and C are same and equal to Δy.

Similar formulas were used in cases where the wet point in the vicinity of the shoreline are on the left side of the shoreline point. In this case backward difference equations were used instead of (5.16).

Chapter 6

RESULTS

In this chapter the results of the nearshore circulation model SHORECIRC, with the implementation of the moving shoreline boundary condition, are compared with the analytical solutions for flow in one horizontal dimension and with the numerical results from other models for flow in two horizontal dimensions. As mentioned in chapter (2), the source terms in the governing equations are neglected in the numerical computations which also makes the numerical results equivalent to the results they are compared with in this chapter. Both the methods of treatment of the moving shoreline, i.e. the coordinate transformation, and a fixed grid with a wet-dry interface, were implemented.

In the one dimensional case, three situations will be simulated. They are, the transient solution and the periodic solution given by Carrier and Greenspan (1958) (CG58 hereafter) and the solution for the run up of a solitary wave given by Synolakis (1987). The bottom topography for both the cases of CG58's solution is a plane sloping beach, where as for the Synolakis (1987) case, topography has a constant depth offshore followed by a plane sloping beach near the shoreline.

As no analytical solutions are available for two dimensional run up, the present model results are compared with the results of other numerical models. The case of a solitary wave run up as described by Zelt (1986) for a concave beach and the simulation of the same case by Özkan Haller and Kirby (1997) are chosen for this purpose.

In the following sections, results will be presented first for the coordinate transformation method and then for the fixed grid with a wet-dry interface method for the boundary condition at the moving shoreline.

6.1 The coordinate transformation method

The comparison of the results of SHORECIRC is presented, with the moving shoreline, treated with a coordinate transformation method as described in chapter (4).

The transformation functions,

$$f(\bar{x}) = (e^{-\alpha(M-\bar{x})} - e^{-\alpha M})/(1 - e^{-\alpha M}) \tag{6.1}$$

and,

$$g'(\bar{x}) = 0.5 + \tanh a(M - \bar{x}) \tag{6.2}$$

and thus,

$$g(\bar{x}) = 0.5(\bar{x} + M) - \frac{1}{a}\log\left[\cosh\left\{a(M - \bar{x})\right\}\right] \tag{6.3}$$

were used in the equation (4.1) and a is calculated by solving

$$0.5M = \frac{1}{a}\log\left\{\cosh(aM)\right\} \tag{6.4}$$

The equation (6.4) was obtain such that the function $g(\bar{x})$ as given in (6.3) satisfies the condition (4.5).

6.1.1 Comparison with analytical solutions in 1DH

Here the comparison of the results for the transient case and the periodic case described by CG58 and for the run-up of a solitary wave as given by Synolakis (1987) will be presented. The analytical solutions are given in terms of the non-dimensional variables. The scalings used were,

$$x^* = x/l \tag{6.5}$$

$$\zeta^* = \zeta/(\alpha l) \tag{6.6}$$

$$u^* = u/\sqrt{g\alpha l} \tag{6.7}$$

$$t^* = t/\sqrt{\alpha l/g} \tag{6.8}$$

where superscript $(\cdot^*)$ represents the non-dimensional value of $(\cdot)$, α is the bottom slope and l is the length scale, which can be selected for the specific problem under investigation.

6.1.1.1 The Carrier and Greenspan's solution : Transient case

The Analytical solution of the Nonlinear Shallow Water equations for plane sloping beaches were obtained by CG58 by using a series of transformations which finally reads as,

$$\sigma^* = 4c^* \tag{6.9}$$

$$\lambda^* = 2(u^* + t^*) \tag{6.10}$$

where c^* is the non-dimensional phase speed which is equal to $\sqrt{d^*}$. More details of the transformations used can be seen in Appendix A.

At the shoreline, the waterdepth $d^* = \zeta^* + h_0^* = 0$, so $c^* = \sqrt{d^*} = 0$ and thus with this transformation, $\sigma^* = 0$ always represents the shoreline position.

The dependent variables x, ζ, t, and u are obtained in terms of the independent variables σ and λ. Appendix A describes the transformations used by CG58, the solutions obtained by them and the reverse transformation which transforms $\zeta(\sigma, \lambda)$, $u(\sigma, \lambda)$, $x(\sigma, \lambda)$, and $t(\sigma, \lambda)$ back to $\zeta(x, t)$ and $u(x, t)$. This is used here to first specify the initial conditions in the model simulations and then to compare the simulation results.

CG58 described some initial value problems and their analytical solution. In the transient case, the initial water surface elevation is assumed to have a depression near the shoreline and it is released from that state of rest. The surface elevation and corresponding x locations in the non-dimensional form are given by,

$$\zeta^* = \epsilon \left[1 - \frac{5}{2} \frac{a^3}{(a^2 + \sigma^2)^{\frac{3}{2}}} + \frac{3}{2} \frac{a^5}{(a^2 + \sigma^2)^{\frac{5}{2}}} \right] \tag{6.11}$$

$$x^* = -\frac{\sigma^2}{16} + \zeta^* \tag{6.12}$$

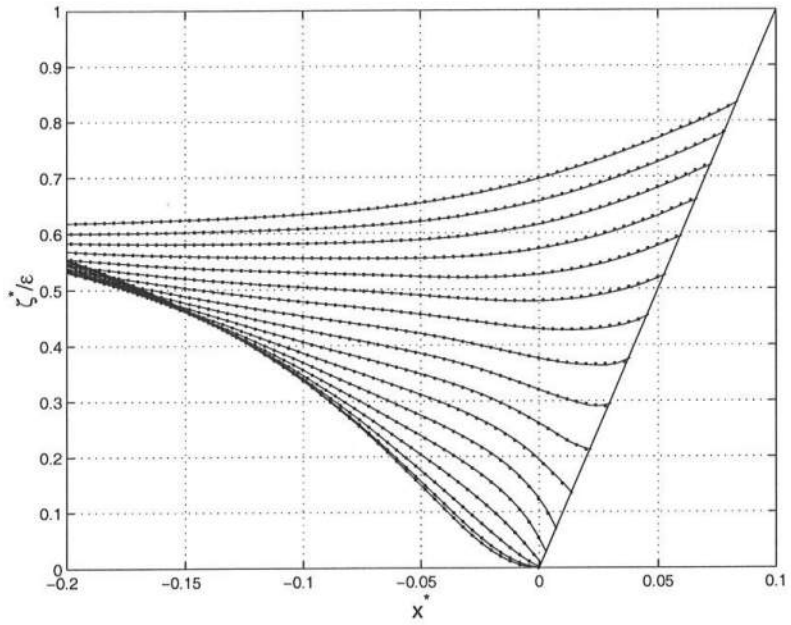

Figure 6.1: SHORECIRC results with the coordinate transformation method for the CG58's transient solution for surface elevation as a function of the cross-shore distance at $t^* = 0$ to $t^* = 0.8$ at the steps of $\Delta t^* = 0.05$. Analytical solution ($\cdots\cdots$); Present model (———). $\Delta \bar{x}^* = 0.007735$ and $\Delta t^* = 0.025$ were used in the simulations.

where,

$$a = 1.5(1 + 0.9\epsilon)^{\frac{1}{2}} \tag{6.13}$$

and initially,

$$u^* = 0 \tag{6.14}$$

Here ϵ is a small parameter, which characterizes the magnitude of the depression. The surface elevation becomes asymptotically equal to ϵ as x goes to infinity offshore and this is the maximum surface elevation. The minimum surface elevation is zero and it occurs at the shoreline at $t^* = 0$. Initial surface profile has a zero tangent at the shoreline and at $x^* = -1$, $\zeta^* = 0.9\epsilon$. For non-breaking cases, the value of ϵ should be less than or equal to 0.23 as predicted by CG58.

The results are presented here for $\epsilon = 0.1$. The bottom slope α is taken to be $1/50$ and the length scale l was selected to be $20m$.

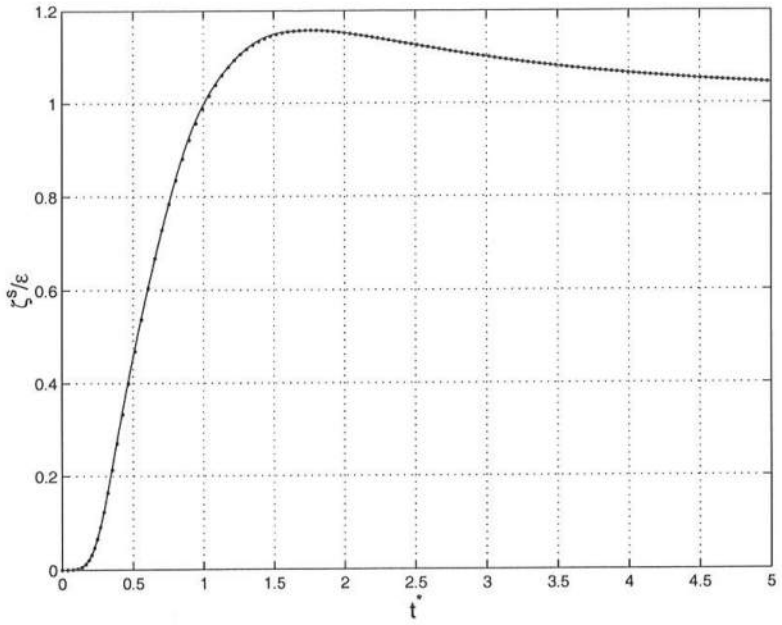

Figure 6.2: SHORECIRC results for the time series of the surface elevation at the shoreline with the coordinate transformation for the CG58's transient solution. Analytical solution ($\cdots\cdots$); Present model (———). $\Delta\bar{x}^* = 0.007735$ and $\Delta t^* = 0.025$ were used in the simulations.

In order to simulate this situation in the present model, the dimensional form of the surface elevation profile, which was obtained by using (6.5) and (6.6) in (6.11) and (6.12), was imposed in the model and the initial velocity field was set to be zero through out the domain.

Figure 6.1 shows the non-dimensional surface elevation as a function of the cross-shore distance x^* at time $t^* = 0$ to $t^* = 0.8$ in steps of $\Delta t^* = 0.05$. Figure 6.2 shows the time series of the non-dimensional surface elevation at the shoreline for t^* upto 5. As can be seen from this figure, the shoreline shoots past the maximum initial surface elevation ϵ and then slowly comes back to asymptotically approach ϵ as time t^* goes to infinity. In both the figures above, surface elevation has been scaled with the depression parameter ϵ. We see that the present model results are in excellent agreement with the analytical solutions.

In the model run for Figure 6.1 and Figure 6.2, $\Delta\bar{x}^*$ was specified to be

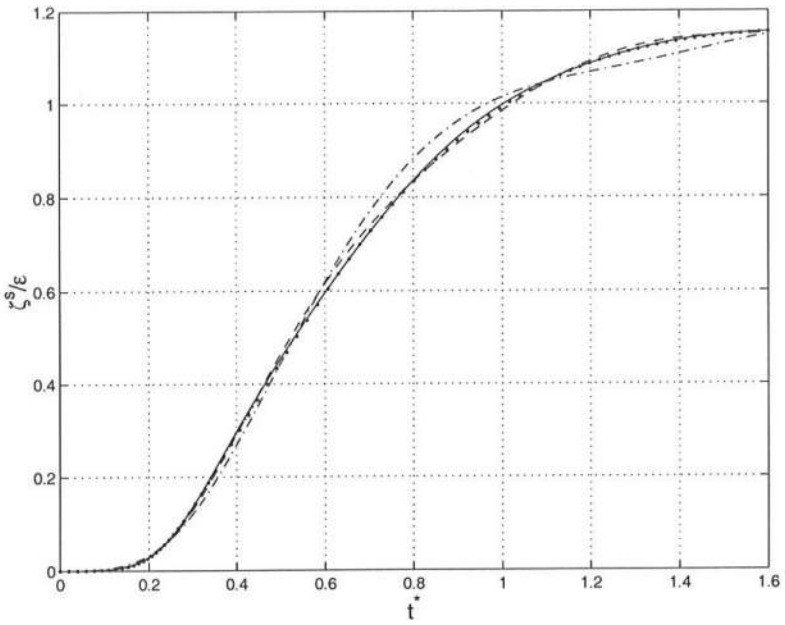

Figure 6.3: Dependence of the numerical solution on grid spacing. Analytical solution (· · ·); $\Delta\bar{x}^* = 0.007735$ (———); $\Delta\bar{x}^* = 0.01547$ (– – –); $\Delta\bar{x}^* = 0.03094$ (–·–·–). Courant no. $Cr = 0.7$ for all the cases

0.007735, the Courant number Cr at the offshore boundary was 0.7 and the corresponding Δt^* was 0.0025. In Figure 6.3 and Figure 6.4 the effect of increase in Δx^* and Δt^* are shown respectively. In these figures, the plots are given for $0 < t^* < 1.6$ as to show how the model results start deviating from the analytical solution. Because of the coordinate transformation, Δx changes with the cross-shore position. However, the computational cost depends on the number of grid points and hence on $\Delta\bar{x}$, thus $\Delta\bar{x}$ has been used here for demonstration of the effects, an increase in the grid spacing has, on the present model results.

In Figure 6.3 the model results are analyzed for sensitivity to the value of Δx^* it can be seen that for $\Delta\bar{x}^* \leq 0.015$, the errors in the model results are small. However, $\Delta\bar{x}^* \cong 0.031$ produces significant deviations in the model results from the analytical solution.

Similarly Figure 6.4 shows the time series of the shoreline position for different

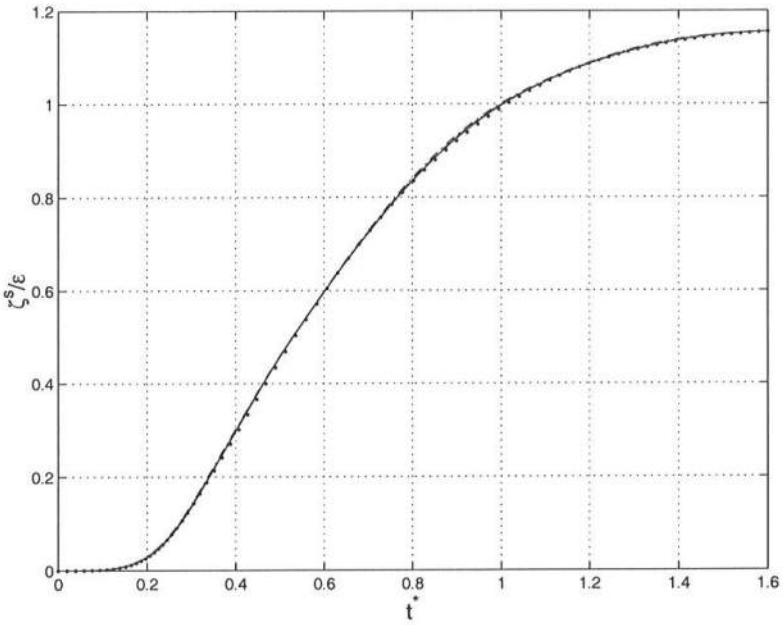

Figure 6.4: Dependence of the numerical solution on time step. Analytical solution (- - -); $Cr = 0.7$ (———); $Cr = 0.9$ (– – –); $Cr = 1.0$ (–·–·–). $\Delta\bar{x}^* = 0.007735$ for all the cases.

values of the Courant number. For all these cases $\Delta\bar{x}^* = 0.007735$. It is clear that only small errors were introduced with the increase of Courant number even upto 1.0 and thus with the increase of Δt^*.

Since in Figure 6.3 the Courant number is constant, a change in $\Delta\bar{x}$ changes Δt also. The results, however, do not depend a lot on Δt as shown by Figure 6.4, so the conclusions that the difference between different curves in Figure 6.3 is only due to change in Δx are well justified.

6.1.1.2 The Carrier and Greenspan's solution : Periodic case

CG58 also presented the analytical solution for the periodic standing waves on a plane sloping beach. For this case, the surface elevation ζ, cross-shore position x, velocity u and time t are given in the non-dimensional form by,

$$\zeta^* = \frac{A}{4} J_0(\sigma^*) \cos\lambda^* - \frac{u^{*2}}{2} \tag{6.15}$$

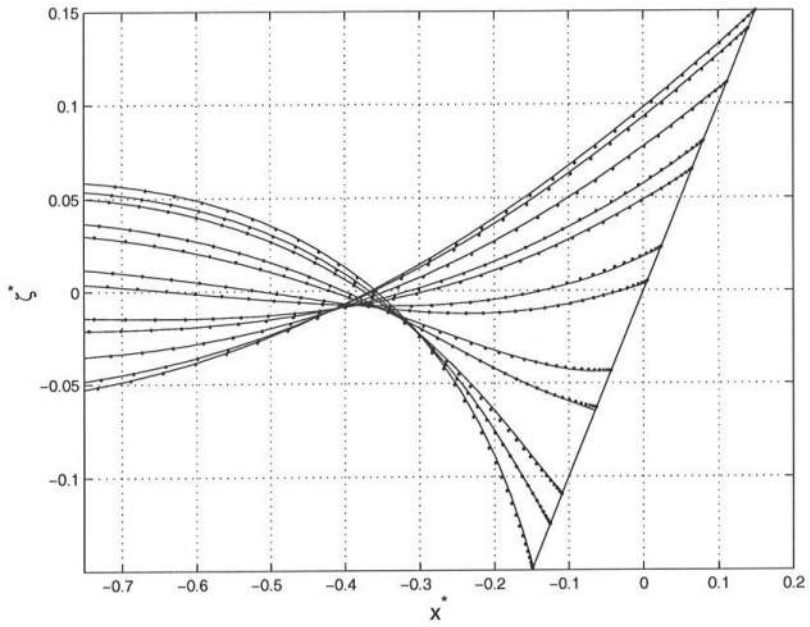

Figure 6.5: The surface elevation as a function of the cross-shore distance at different time steps for the periodic solution. The coordinate transformation model (———); Analytical solution (- - -). $\Delta\bar{x}^* = 0.0647$ and Courant number $Cr = 0.7$ were used.

$$x^* = -\frac{\sigma^{*2}}{16} + \zeta^* \tag{6.16}$$

$$u^* = -\frac{AJ_1(\sigma^*)\sin\lambda^*}{\sigma^*} \tag{6.17}$$

$$t^* = \frac{1}{2}\lambda^* - u^* \tag{6.18}$$

This represents a wave of non-dimensional frequency equal to one, traveling towards the shore, getting fully reflected from there and creating a standing wave like situation.

Here A is the non-dimensional wave amplitude. $A/4$ is the maximum vertical excursion of the shoreline. The above solution is valid for $0 \leq A \leq 1$. $A = 1$ corresponds to a vertical tangent on the surface elevation. Mathematically, when $A = 1$, the Jacobian of the transformation used to arrive at these solutions becomes zero and the transformation looses the one-to-one correspondence between the actual

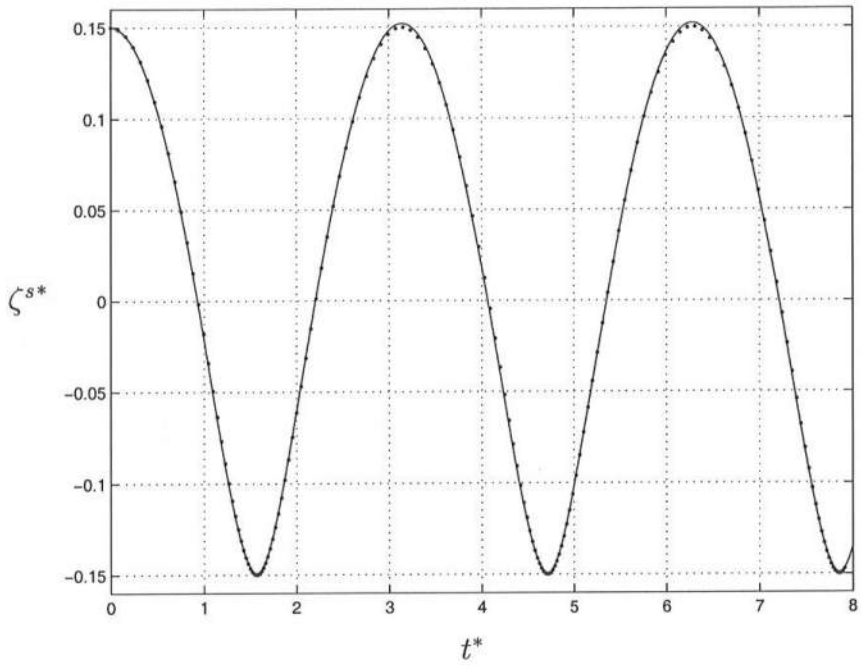

Figure 6.6: The time series of the surface elevation at the shoreline for CG58 periodic case. The coordinate transformation model (———); Analytical solution (- - -). $\Delta\bar{x}^* = 0.0647$ and Courant number $Cr = 0.7$ were used.

and the transformed variables.

At $\lambda = 0$, we have $u^* = 0$ and $t^* = 0$. So, the initial conditions are given here by,

$$\zeta^* = \frac{A}{4} J_0(\sigma) \tag{6.19}$$

$$x^* = -\frac{\sigma^2}{16} + \zeta^* \tag{6.20}$$

and

$$u^* = 0 \tag{6.21}$$

In this case also, the initial condition of the surface elevation was imposed on the numerical model by using (6.6) and (6.5) to obtain the dimensional form of (6.19) and (6.20). The initial velocity field was set to be zero.

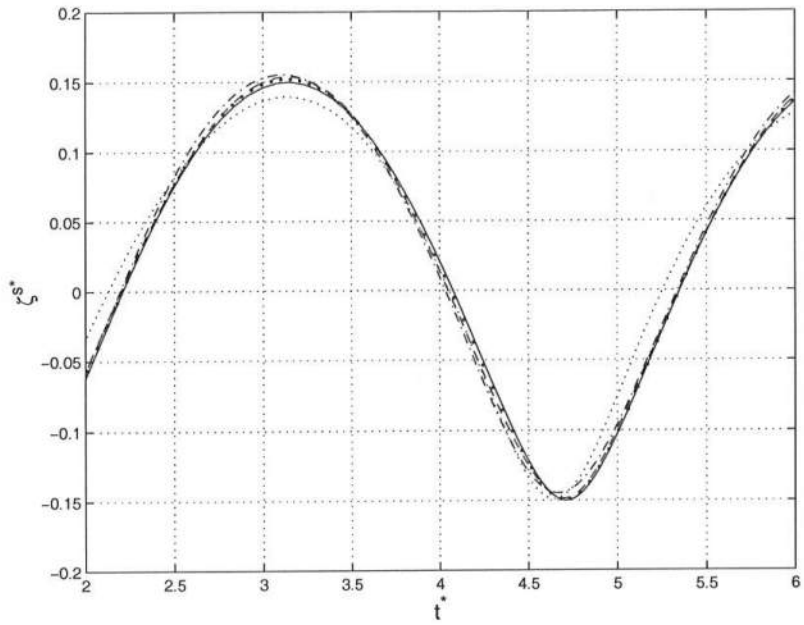

Figure 6.7: Effect of increase in grid spacing for CG58 periodic case. Analytical solution (———); $\Delta\bar{x}^* = 0.032345$ (· - ·); $\Delta\bar{x}^* = 0.06469$ (– – –); $\Delta\bar{x}^* = 0.12938$ (–·–·–); $\Delta\bar{x}^* = 0.25876$ (· · · · ·). $Cr = 0.7$ for all the cases.

The length scale $l = 20m$ and the bottom slope α was chosen to be 1/30. Results for $A = 0.6$ are presented here. $\Delta\bar{x}^* = 0.0647$, which results in about 10 points from the shoreline to the first "node" in surface elevation, and the Courant number $Cr = 0.7$ were used in this case.

Figure 6.5 shows the non-dimensional surface elevation as a function of the cross-shore position x^* at different time t^*. Figure 6.6 shows the time series of the non-dimensional surface elevation at the shoreline. Again, the model compares well with the analytical solution. Figure 6.6 shows a very small deviation of the model result from the analytical result at the maximum and minimum shoreline run-up.

Figure 6.7 shows the time series of the surface elevation at the shoreline for different grid spacing. Similar to the transient case, here also $\Delta\bar{x}^*$ is used as a measure of grid spacing. It can be concluded from this figure that for $\Delta\bar{x}^* \leq 0.13$, the results are very accurate. However for $\Delta\bar{x}^* \cong 0.26$, the errors get significantly larger.

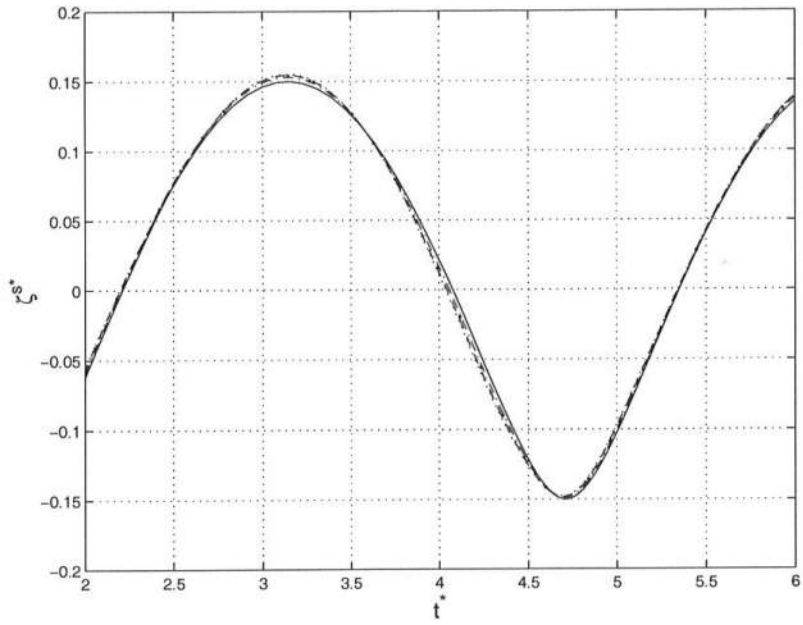

Figure 6.8: Effect of increase in time step for CG58 periodic case. Analytical (———); $Cr = 0.5$ (–·–·–); $Cr = 0.7$ (· · ·); $Cr = 0.9$ (– – –); $Cr = 1.0$ (· · · · ·). $\Delta\bar{x}^* = 0.0647$ for all the cases.

Figure 6.8 shows the time series of the surface elevation at the shoreline for different Δt^* which is obtained by using different Courant numbers. As observed, the results do not change a lot with increase in Δt as long as the Courant number is below 1. As the time step is calculated using the Courant number at the offshore boundary, increasing it above 1.0 starts numerical instabilities at the offshore boundary which soon covers the complete domain.

6.1.1.3 Run-up of a solitary wave

Synolakis (1987) derived an analytical solution for the run-up of a first order solitary wave. Figure 6.9 shows the bottom topography and the different parameters of the incident solitary wave. The bottom topography has a constant waterdepth offshore and a plane sloping beach near the shoreline. These two parts meet at $x^* = {X_0}^*$.

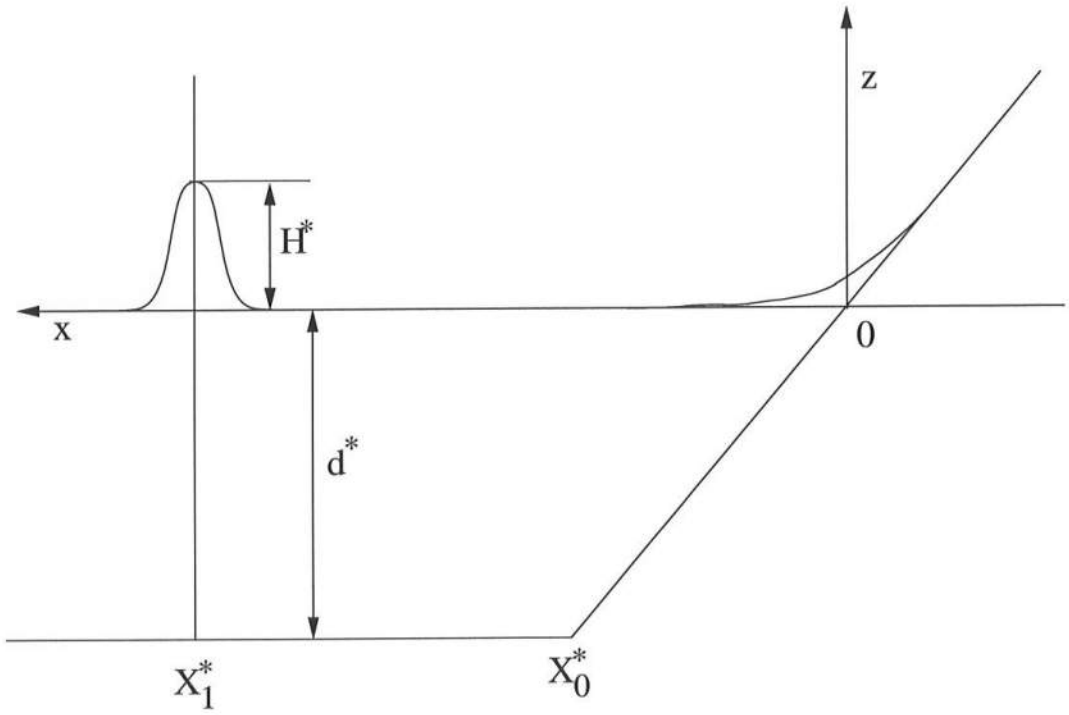

Figure 6.9: Definition sketch for Synolakis' solution of a solitary wave run-up

The peak of the solitary wave used here, is initially at $x^* = X_1^*$, and the initial surface profile is given by,

$$\zeta^* = \frac{H^*}{d^*}\text{sech}^2\left\{\sqrt{\frac{3H^*}{4d^*}}(x^* - X_1^*)\right\} \tag{6.22}$$

This is the profile for a first order solitary wave so this waveform will represent a solitary wave only when the wave height is small. Since the NSW equations were used here and the dispersion terms were not included, the initial waveform will not preserve it's form even on a horizontal bottom. However, Synolakis' analytical result was also obtained for the NSW equations, so the numerical results obtained here are equivalent to the results obtained by Synolakis (1987).

Synolakis (1987) used $H^*/d^* = 0.019$ and the beach slope $\alpha = 1/19.85$ in order to compare experimental results with the analytical solution. In the present numerical model simulations, we used the same values.

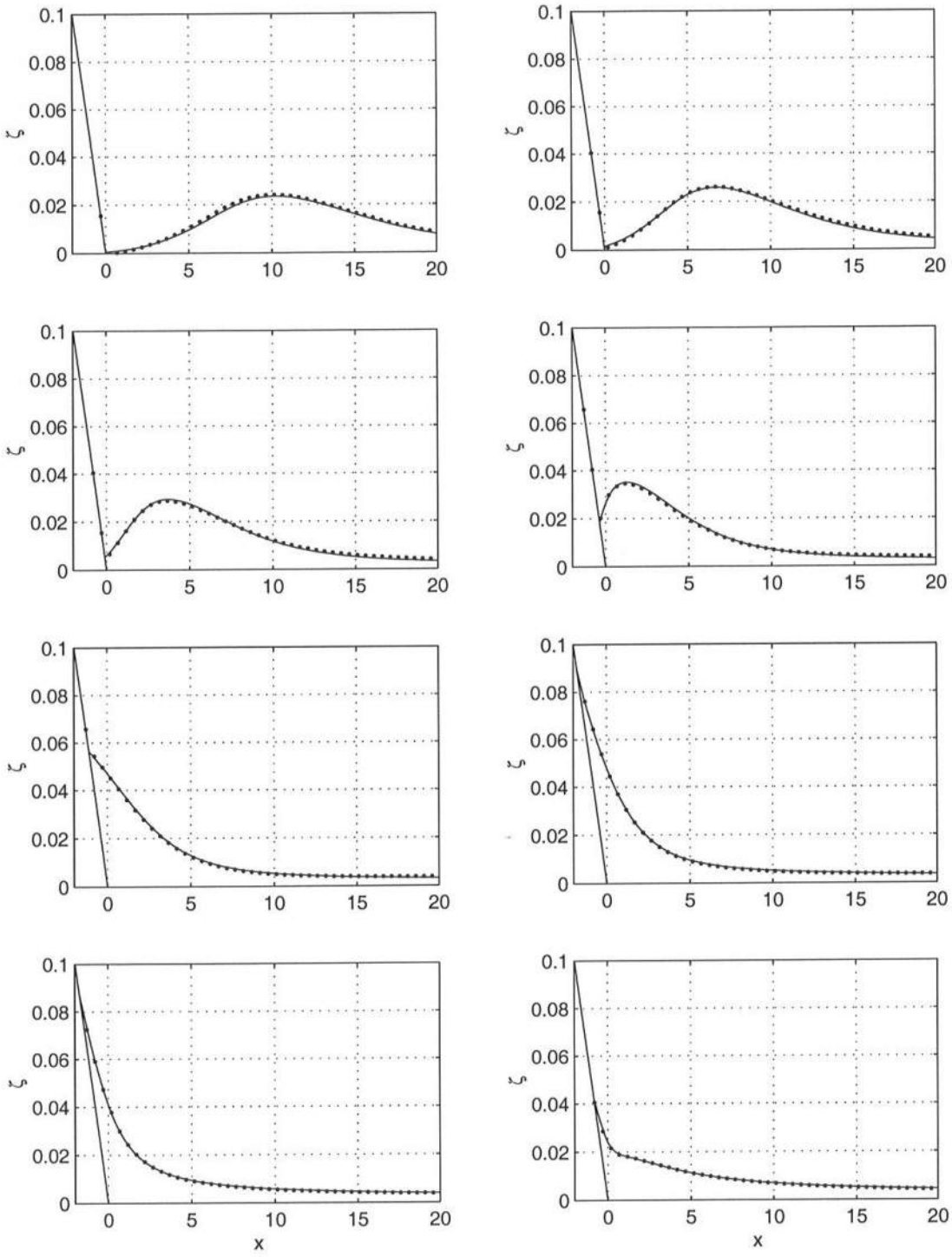

Figure 6.10: Run-up of a solitary wave. Analytical solution (- - -); the coordinate transformation model (———).

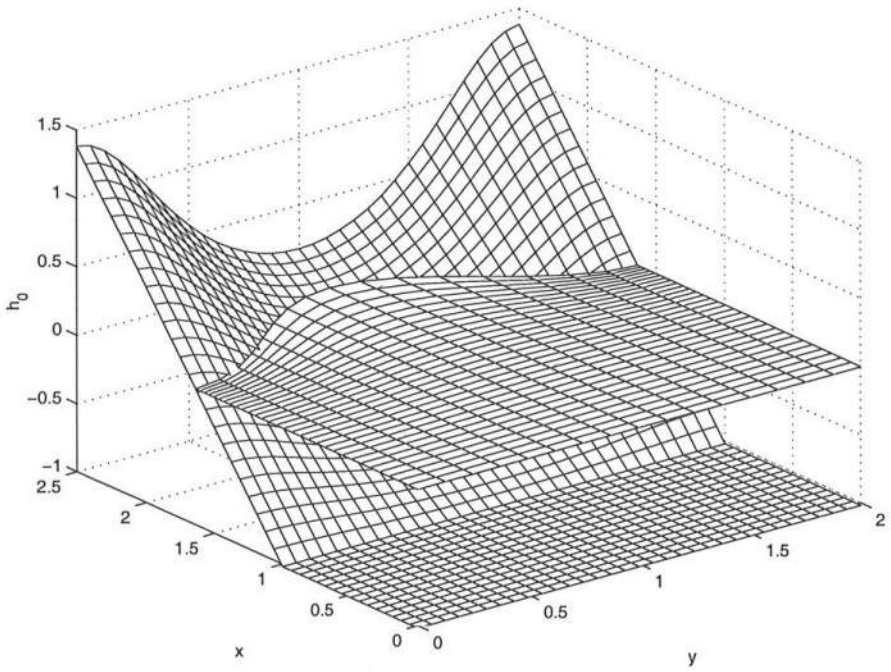

Figure 6.11: Bottom topography used by Zelt (1986)

Figure 6.10 presents a comparison with the coordinate transformation method for the surface elevation ζ^* as a function of the cross-shore distance x^* at times $t^* = 20$ to $t^* = 55$ in the steps of $\Delta t^* = 5$. We see that the model predictions are in good agreement with the analytical results even at time $t^* = 45$, the approximate time of maximum run-up. In the case shown here, $\Delta \bar{x}^* = 0.2$ and Courant number $Cr = 0.7$ were used.

6.1.2 Comparison with numerical solutions in 2DH

In the course of studying the response of harbors to long wave excitation, Zelt (1986) developed a Lagrangian finite element model. It was applied to the case of the run-up and run-down due to the incidence of a solitary wave on a beach where a curved shoreline meets a region of constant depth with a sloping bathymetry nearshore. The bottom topography is shown in the Figure 6.11. Such geometry was chosen to demonstrate the interaction of different processes affecting the shoreline

run-up. This case is used here for comparison with the results of the coordinate transformation model in 2DH.

The undisturbed waterdepth, as shown in Figure 6.11, is given by,

$$h(x,y) = \begin{cases} h_0, & \text{for x < L} \\ h_0 - \frac{h_0\pi}{L}\left[\frac{(x-L)}{3-\cos\left(\frac{\pi y}{L}\right)}\right]. & \text{for x} \geq \text{L} \end{cases} \tag{6.23}$$

where the length scale L is half the wavelength of the cosine form of the shoreline.

By setting $h = 0$ in (6.23) and solving for x, the initial shoreline position can be obtained and is given by,

$$x^s = L + \frac{L}{\pi}\left(3 - \cos\frac{\pi y}{L}\right) \tag{6.24}$$

As oppposed to Synolakis' case, where the initial profile of the solitary wave was prescribed, here the incident solitary wave was introduced at the offshore boundary of the model domain. In this case, the incident wave, as described in VanDongeren and Svendsen (1997b), was given as,

$$\zeta^o(t) = \frac{H}{h_o}\text{sech}^2\left\{\left(\sqrt{\frac{3\alpha}{4\beta}(1+\alpha)}\right)(t-t_0)\right\} \tag{6.25}$$

where $\zeta^o(t)$ is the surface elevation at the offshore boundary, $\alpha = H/h_o$ is the nonlinearity parameter and $\beta = (h_0/L)^2$ is the dispersion parameter. t_0 was obtained such that the initial surface elevation at the offshore boundary was 1% of the wave height. It was observed by Zelt (1986) that $\alpha \geq 0.3$ results in a vertical tangent developing on the surface elevation during the run-down which means that the assumptions behind the equations fail, which leads to numerical problems. This situation is similar to the case of $A = 1$ for the periodic case in the Carrier and Greenspan solution in one horizontal direction. $\alpha = 0.2$ was selected for the present model comparisons.

From (6.23) the bottom slope is given by,

$$h_x(y) = \frac{h_0\pi}{L}\frac{1}{\left\{3 - \cos\left(\frac{\pi y}{L}\right)\right\}} \tag{6.26}$$

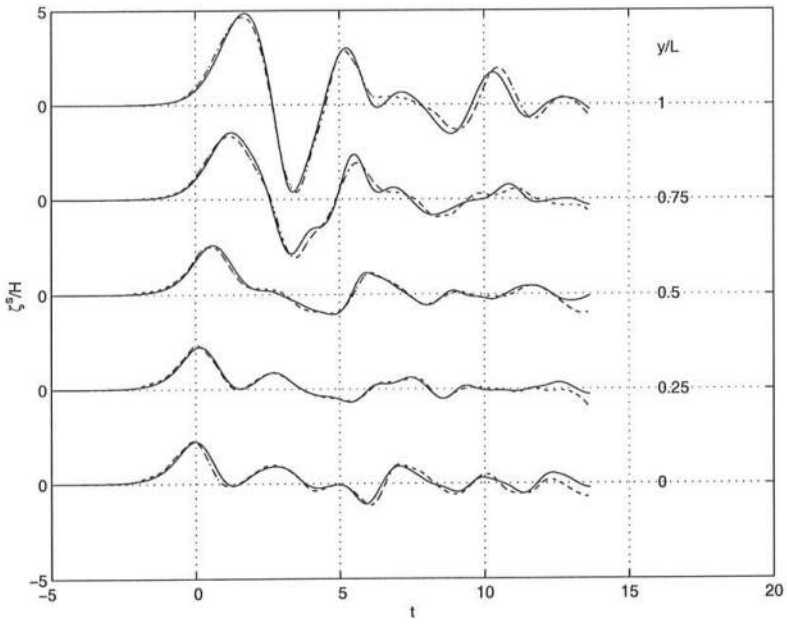

Figure 6.12: Time series of the surface elevation at the shoreline along different longshore locations. The present model (———); Zelt (1986) (– · – · –).

In the model domain, the slope changes from 1/5 at the lateral boundaries of the domain ($y = 0$ and $y = 2L$) to 1/10 at the center ($y = L$). On substituting these values in (6.26),

$$\frac{1}{10} = \frac{h_0 \pi}{L} \frac{1}{\{3 - \cos(\pi)\}} \tag{6.27}$$

or,

$$\beta = \left(\frac{h_0}{L}\right)^2 = \left(\frac{4}{10\pi}\right)^2 = 0.0162 \tag{6.28}$$

Since the incident solitary wave was introduced in the domain through the offshore boundary, an absorbing-generating boundary condition as described by Van-Dongeren and Svendsen (1997a) was used at the offshore boundary.

6.1.2.1 Zelt (1986)'s case

The results of the simulations by Zelt (1986) for the topography shown in Figure 6.11 were presented as the time series of the surface elevation of the shoreline

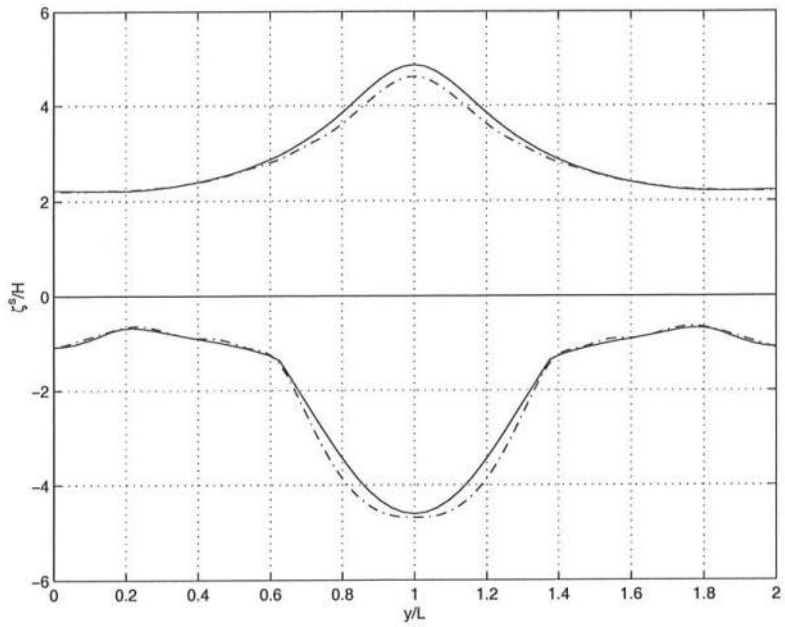

Figure 6.13: The maximum run-up and the minimum run-down as a function of the longshore position. The present model (———); Zelt (1986) (– – – –).

at the five locations, $y/L = 0, 0.25, 0.5, 0.75, 1$ in the longshore direction and the maximum run-up and run-down as a function of the longshore position for the different values of α. Time has been non-dimensionalized with a time scale $T = \sqrt{gh_0}/L$ and the non-dimensional time $t = 0$ is chosen as the time at which the run-up is maximum at the lateral boundaries.

Figure 6.12 shows the comparison between Zelt (1986) results and the results for the coordinate transformation method for time series of surface elevation at the five locations. Figure 6.13 similarly shows the comparison for the maximum run-up and the minimum rundown predicted by the coordinate transformation model to the results presented by Zelt (1986). $\Delta\bar{x}^* = 0.01278$ and Courant number $Cr = 0.7$ were used in the present model simulations.

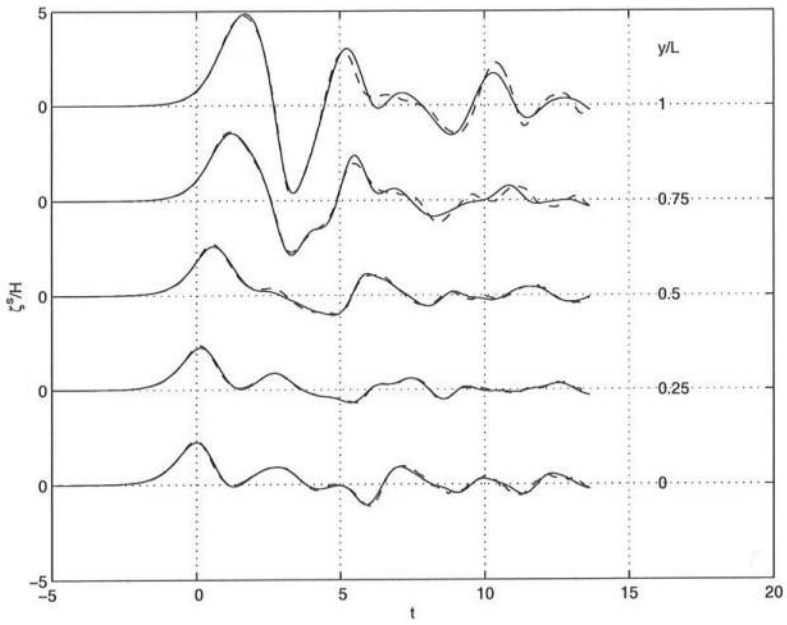

Figure 6.14: Time series of the surface elevation at the shoreline along different longshore locations. The present model (———); Özkan Haller and Kirby (1997) (– – –).

6.1.2.2 Özkan Haller and Kirby (1997)'s simulation of Zelt's case

Özkan Haller and Kirby (1997) also used Zelt's case to test the moving shoreline boundary condition in 2DH, for their Fourier-Chebyshev collocation model. The results of the present model compared with those obtained by Özkan Haller and Kirby (1997) are shown in Figure 6.14, again as the time series of the surface elevation at the five stations. Figure 6.15 shows the maximum run-up and the minimum run-down along the longshore direction obtained from the two models.

It is seen that the coordinate transformation model compares quite well with the results of both, Zelt (1986) and Özkan Haller and Kirby (1997). It's prediction of the first run-up peak is in very good agreement with the other two models. The present model starts deviating from the Zelt's solution at about non-dimensional time $t = 12$. In general it is in a better agreement with the solution given by Özkan Haller and Kirby (1997). This is apparent from the comparison of Figures 6.13

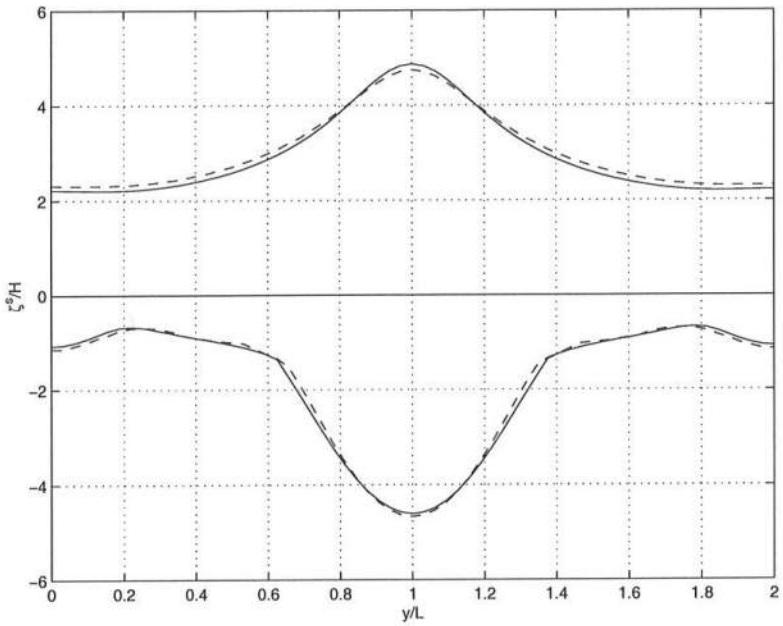

Figure 6.15: The maximum run-up and the minimum run-down as a function of the longshore position. The present model (———); Özkan Haller and Kirby (1997) (– – –).

and 6.15 which show the maximum run-up and the minimum run-down as a function of the longshore distance.

All the results shown here are obtained by numerical simulations and they all are quite close to each other thus it's difficult to say which one is the best. The values of Δx and Δt are not known for the computations of either Zelt (1986) or Özkan Haller and Kirby (1997). Özkan-Haller and Kirby had 128 grid points in the cross-shore direction and 48 in the longshore direction. However due to different coordinate transformation schemes, even when the number of grid points used in the present model is same as the one used by Özkan-Haller and Kirby, the grid size distribution isn't the same as the one used by them. Furthermore the behavior of the other two models with changes in Δx and Δt is not known. This makes further comparative study more difficult. However, it was observed that with a further decrease in grid spacing, the results obtained with the present model doesn't change

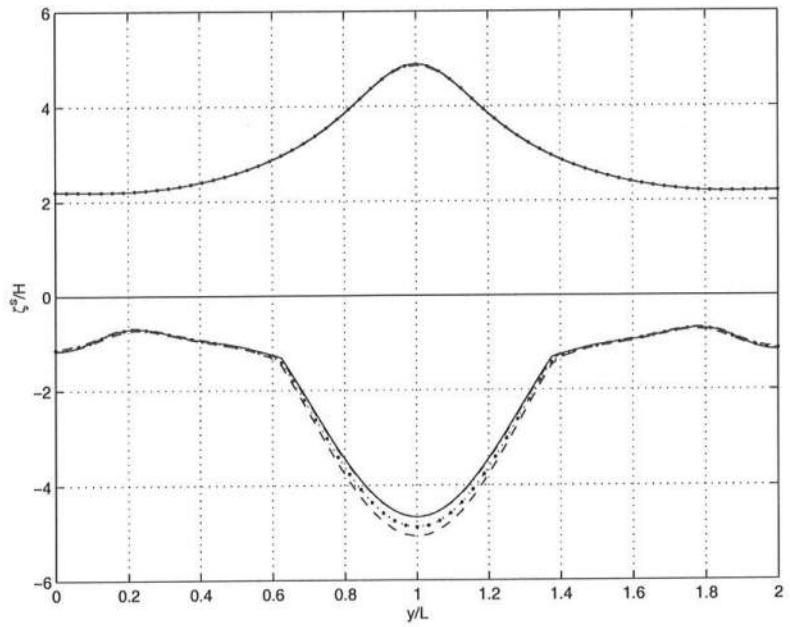

Figure 6.16: The maximum run-up and the minimum run-down as a function of the longshore position for different $\Delta\bar{x}^*$ in the present model. $\Delta\bar{x}^* = 0.01278$ (———); $\Delta\bar{x}^* = 0.0205$ (– – –); $\Delta\bar{x}^* = 0.0273$ (–·–·–); $\Delta\bar{x}^* = 0.041$ (· · ·). Courant number $Cr = 0.7$ for all the cases.

as shown in Figure 6.16. Hence it can be concluded here that for the given Δx and Δt values, all the three models are in good agreement with each other and as the results don't change with further decrease in $\Delta\bar{x}$ in the present model, this result is probably accurate.

Figure 6.17 shows a 3D representation of the surface elevation on the whole domain at different stages of incidence, run-up and run-down of the incoming solitary wave. It is interesting to notice that in spite of the fact that a solitary has no negative surface elevation the run-up process in this topography results in quite large depression of the shoreline at later stages of the process (as could also be seen from the previous figures).

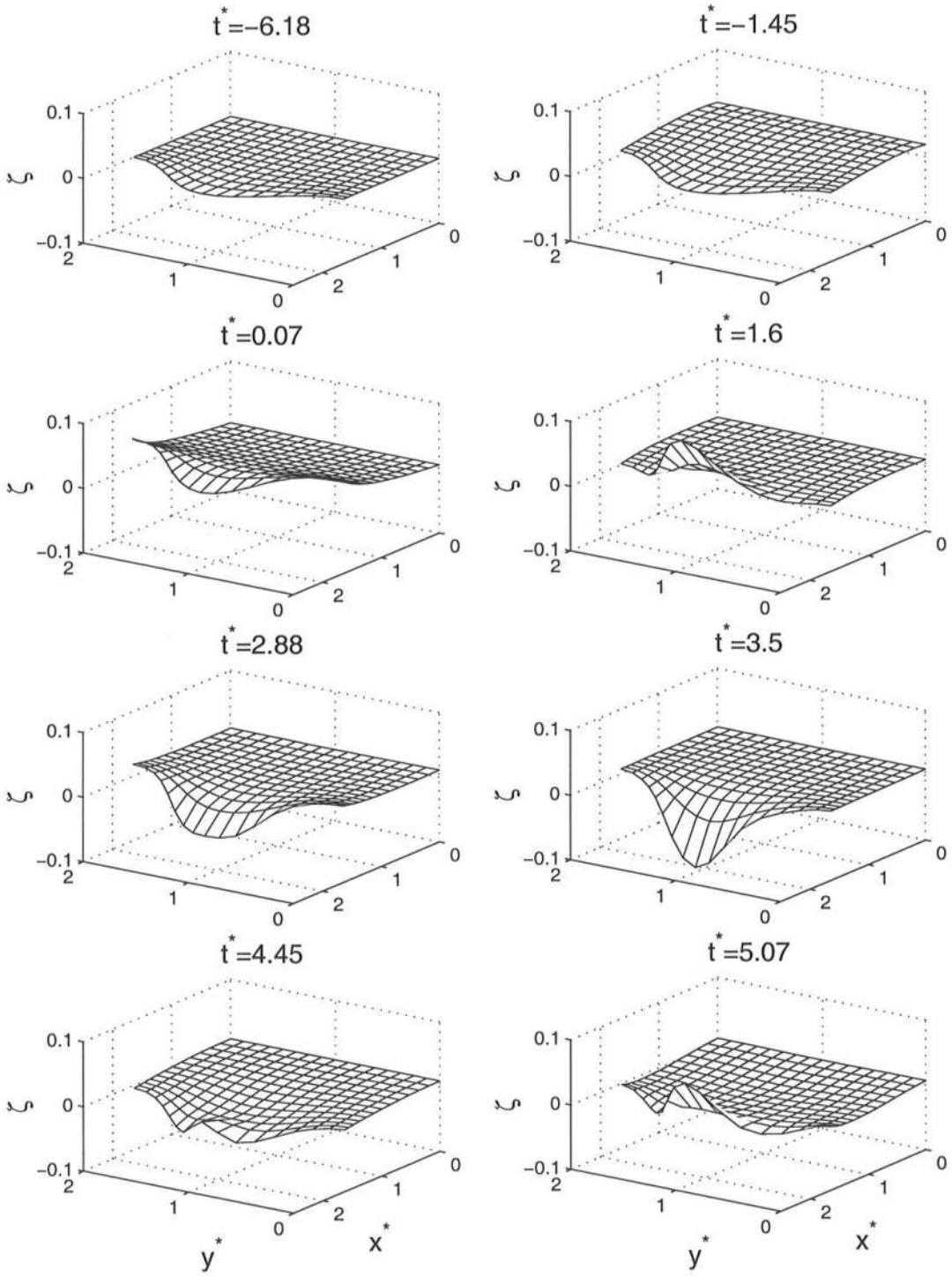

Figure 6.17: The surface elevation over the whole domain as obtained by the coordinate transformation method for the 2DH case.

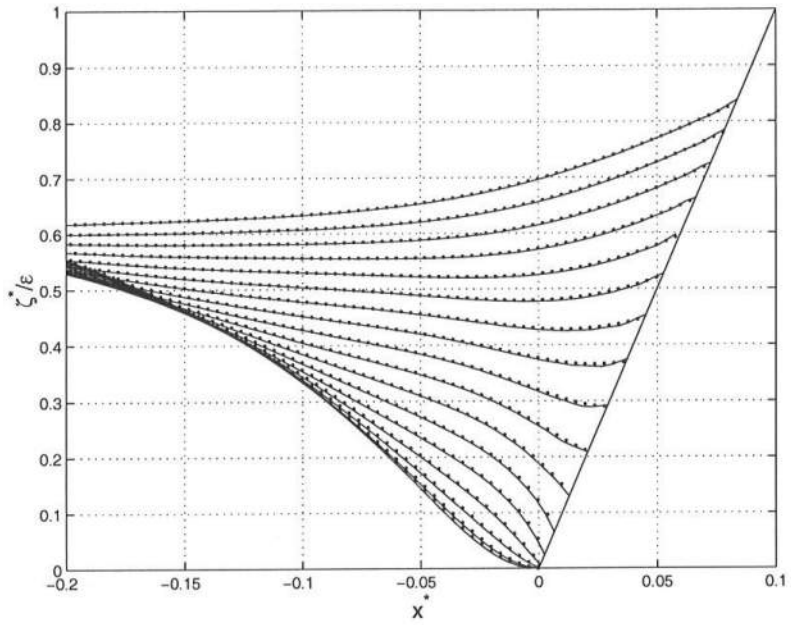

Figure 6.18: Surface elevation as a function of the cross-shore distance at different time steps for the CG58's transient case. The analytical solution (- - -); SHORECIRC with fixed grid (———).

6.2 Shoreline model with fixed grid and wet-dry interface

In this section, the results of the model simulations will be presented for the boundary condition with a fixed grid and a wet-dry interface as described in chapter (5). The cases used for comparison here are the same as the ones used earlier to show the performance of the coordinate transformation method for the treatment of the moving shoreline.

6.2.1 Comparison in 1DH cases

As before the scales used to non-dimensionalize the dependent and independent variables are the same as given by (6.5), (6.6), (6.7) and (6.8).

6.2.1.1 The Carrier and Greenspan's solution : Transient case

The initial surface elevation profile is again given by in non-dimensional form by (6.11) and (6.12). The initial velocity field is set to be zero. The length scale

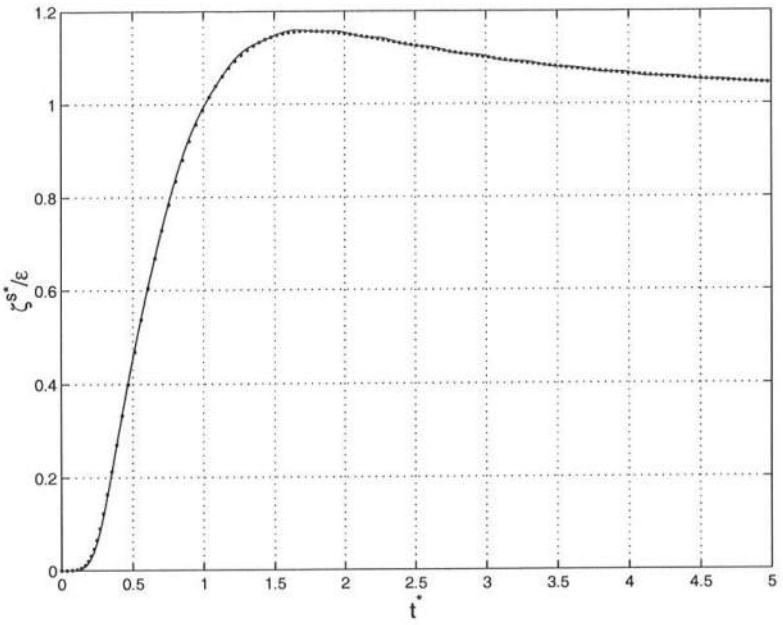

Figure 6.19: Time series of the surface elevation at the shoreline for CG58's transient case. The analytical solution (- - -); SHORECIRC with fixed grid (———).

$l = 20m$ and bottom slope $\alpha = 1/50$ was again selected.

Figure 6.18 shows the result of the surface elevation as a function of the cross-shore distance x^* at time $t^* = 0$ to $t^* = 0.8$ at steps of $\Delta t^* = 0.05$. Figure 6.19 shows the time series of the surface elevation at the shoreline. The surface elevation has been scaled by ϵ, and $\epsilon = 0.1$ was used in this case also.

We see that the fixed grid model predicts the analytical solution very well. The grid spacing used in this case is $\Delta x^* = 0.0039175$, where as $\Delta \bar{x}^* = 0.0077$ was used in the corresponding case with the coordinate transformation method. Since the transformation results in a grid spacing near the shoreline to be $0.5\Delta\bar{x}$, these values imply that near the shoreline the grid spacing was the same in the two examples. Thus it can be concluded that, for the chosen Δx values, the accuracy of the solution in either method of implementation of the moving shoreline is similar and very high.

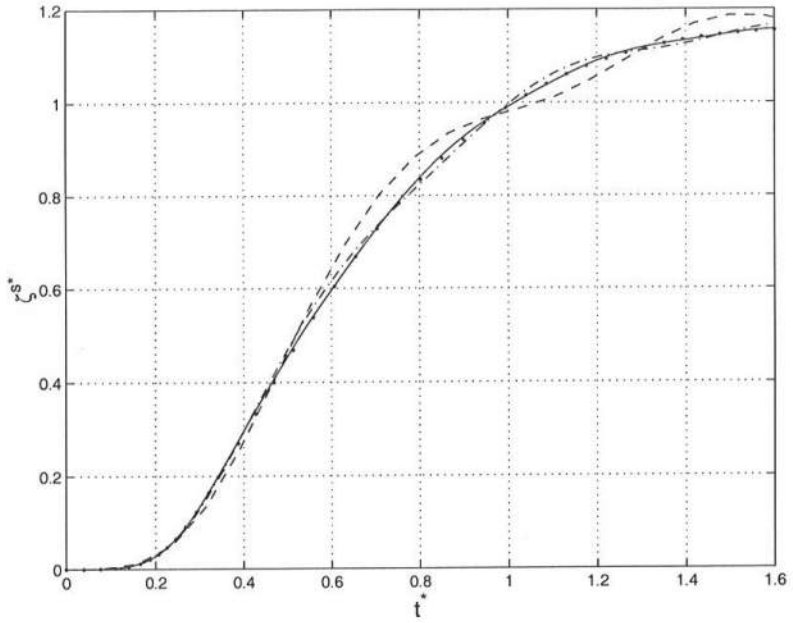

Figure 6.20: Time series of the surface elevation at the shoreline for the CG58's transient case for different Δx^*. The analytical solution (- - -); $\Delta x^* = 0.0039175$ (———); $\Delta x^* = 0.007835$ (– – –); $\Delta x^* = 0.01567$ (–·–·–). Courant number $Cr = 0.7$ for all the cases.

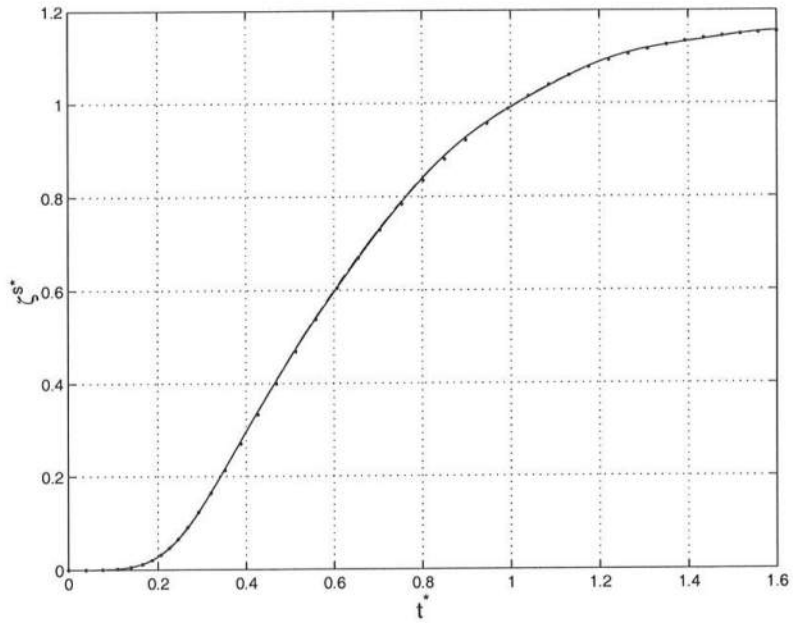

Figure 6.21: Time series of the surface elevation at the shoreline for the CG58's transient case for different values of Courant number. The analytical solution (- - -); $Cr = 0.7$ (———); $Cr = 0.9$ (– – –); $Cr = 1.0$ (–·–·–). $\Delta x^* = 0.007835$ for all the cases.

Figure 6.20 shows the time series of the surface elevation at the shoreline for different Δx^*. The Courant number for all these cases were 0.7. Similarly Figure 6.21 shows the time series of the surface elevation at the shoreline for different Courant numbers. For all these cases Δx^* was 0.0039175. Similar to the case with the coordinate transformation method, here also results deviate more from the analytical with increase in grid spacing than with increase in time steps.

It was observed that for the coordinate transformation method, a $\Delta \bar{x}^* \geq 0.031$ results in larger deviations of the results from the analytical solution, and equivalently with the fixed grid method, a $\Delta x^* \geq 0.016$ results in similar larger errors in numerical simulations. As mentioned these Δx values corresponds to equivalent grid spacing near the shoreline. However as the coordinate transformation method results in larger grid spacing offshore, it requires lesser number of grid points to model a domain that the number of points required to model same domain with the fixed grid method.

6.2.1.2 The Carrier and Greenspan's solution : Periodic case

Similarly for the periodic case, the initial surface profile as given by (6.19) and (6.20) was imposed in the numerical model in the dimensional form. The length scale l was selected to be $20m$ and the beach slope $\alpha = 1/30$. Figure 6.22 shows the surface elevation as a function of the cross-shore distance at different time steps. Figure 6.23 shows the time series of the surface elevation at the shoreline.

The periodic case also requires a Δx^* which is about half the value of $\Delta \bar{x}^*$ used to obtain similar accuracy in the results with the coordinate transformation method. As before this can be attributed to the fact the the coordinate transformation results in reducing the grid spacing near the shoreline to about half the value of $\Delta \bar{x}^*$. So, $\Delta x^* = 0.032345$, used in Figure 6.22 and 6.23, and $\Delta \bar{x}^* = 0.647$, which is used in the corresponding case with the coordinate transformation method, have

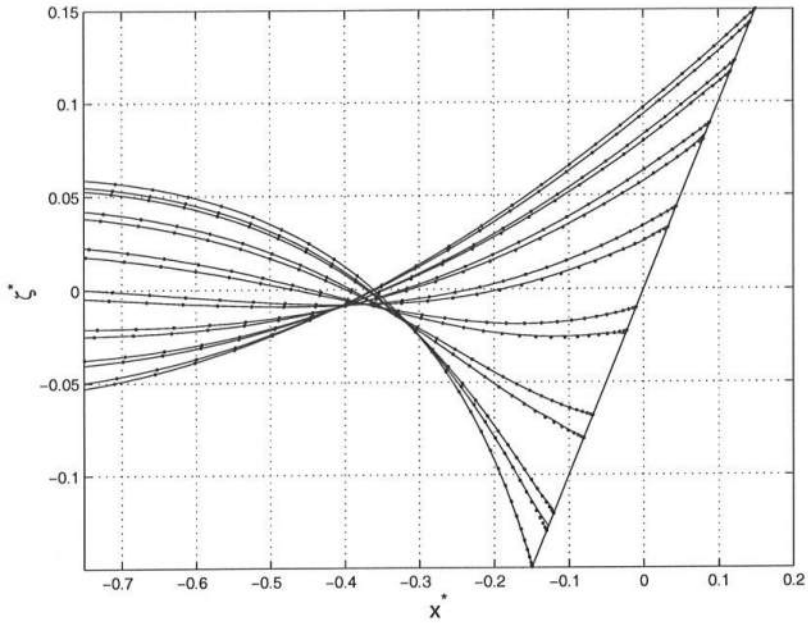

Figure 6.22: The surface elevation as a function of the cross-shore distance at different time steps for the CG58's periodic case. The analytical solution (- - -); SHORECIRC with fixed grid (———).

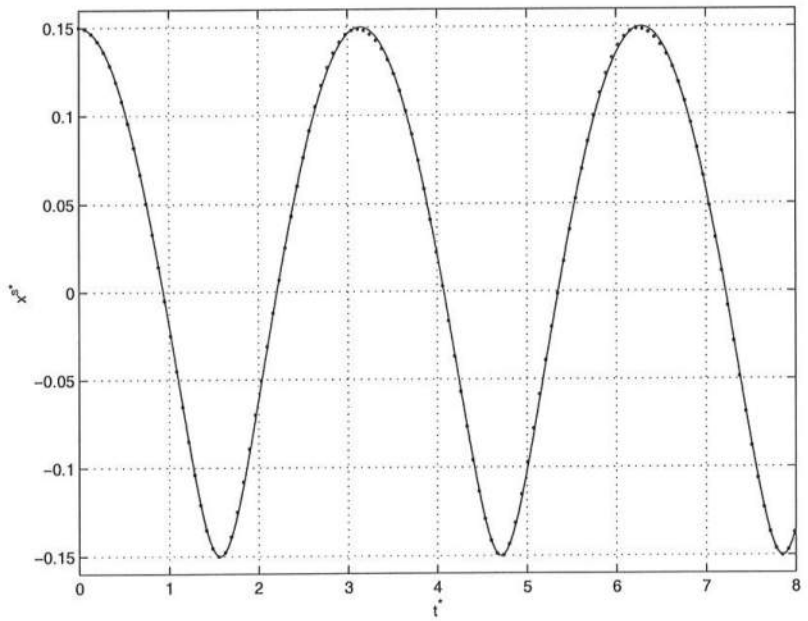

Figure 6.23: Time series of the surface elevation at the shoreline for CG58's periodic case. The analytical solution (- - -); SHORECIRC with fixed grid (———).

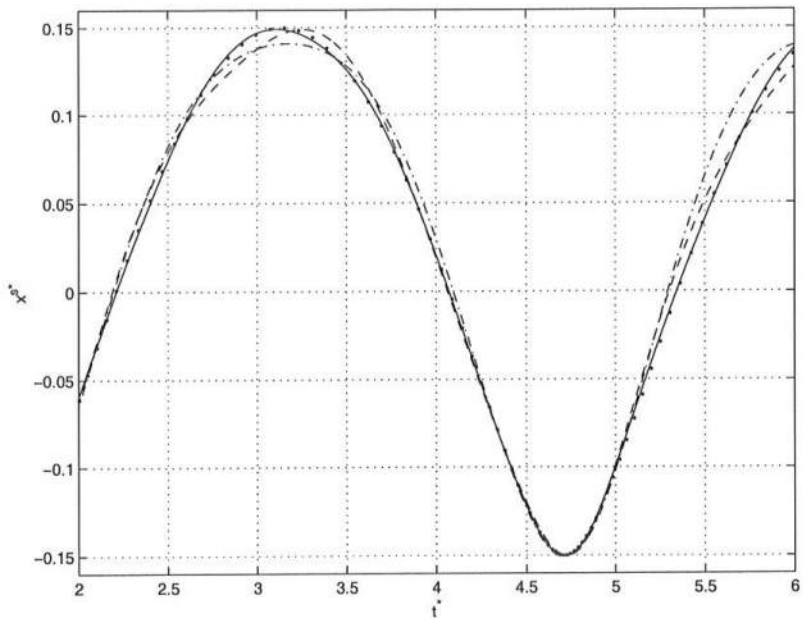

Figure 6.24: Time series of the surface elevation at the shoreline for the CG58's periodic case for different Δx^* in the present model with fixed grid. The analytical solution (· · ·); $\Delta x^* = 0.015$ (———); $\Delta x^* = 0.02$ (– – –); $\Delta x^* = 0.03$ (–·–·–). Courant number $Cr = 0.7$ for all the cases.

a similar resolution near the shoreline. It appears that for the chosen Δx values the two methods give similar and very high accuracy.

Figure 6.24 shows the time series of the surface elevation at the shoreline for different Δx^* in the model with fixed grid. Figure 6.25 shows the time series of the surface elevation at the shoreline for different Courant number in the model. It can be observed that the model starts deviating from the analytical solution with increase in grid spacing and it is seen that this devation is distributed somewhat differently from the deviation observed with the coordinate transformation method for the similar grid spacing in Figure 6.7. However, an increase in time step in Figure 6.25, does not introduce any error similar to the case with the coordinate transformation method in Figure 6.8.

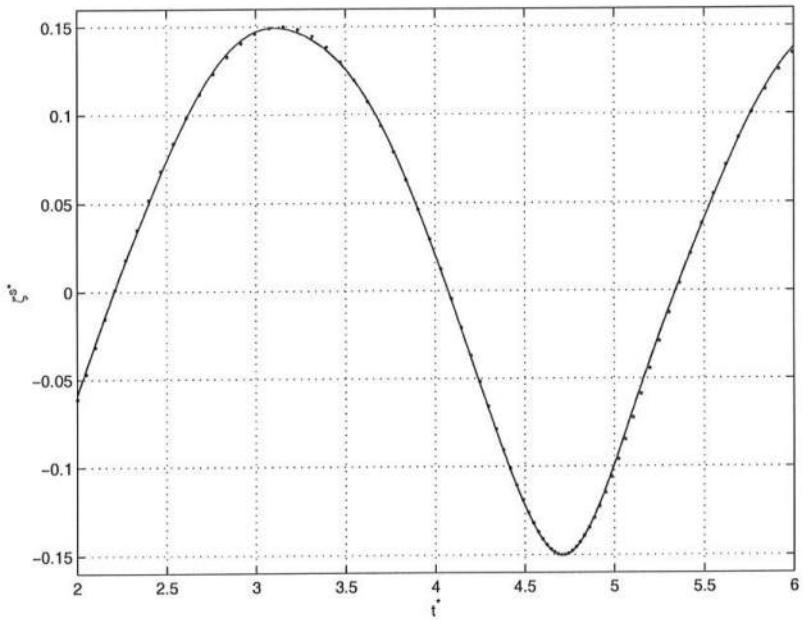

Figure 6.25: Time series of the surface elevation at the shoreline for the CG58's periodic case for different Δx^* in the present model with fixed grid. The analytical solution (· · ·); $Cr = 0.5$ (———); $Cr = 0.7$ (– – –); $Cr = 1.0$ (–·–·–). $\Delta x^* = 0.015$ for all the cases.

6.2.1.3 Run-up of a solitary wave

Figure 6.26 shows the comparison of SHORECIRC results using fixed grids for the case of solitary wave run-up with the analytical solution given by Synolakis (1987). Here the surface elevation is plotted as a function of the cross-shore distance at time $t^* = 20$ to $t^* = 55$ in steps of $\Delta t^* = 5$. $\Delta x^* = 0.1$, again half the value used for the coordinate transformation method and the Courant number is again $Cr = 0.7$ were used in the model simulation. All other parameters are also the same as the ones used in the coordinate transformation method to include a moving shoreline. As Figure 6.26 shows the results are again in excellent agreement with Synolakis' solution.

6.2.2 Comparison in 2DH cases

Similarly, in the two dimensional case, the results of the fixed grid model are compared with Zelt (1986) and Özkan Haller and Kirby (1997)'s model results.

Figure 6.27 shows the comparison of the time series of the surface elevation at the five longshore locations. Figure 6.28 shows the comparison for the maximum run-up and the minimum run-down as a function of the longshore position as obtained by the fixed grid model to the results presented by Zelt (1986). Figure 6.29 and 6.30 show the same results compared to the results obtained by Özkan Haller and Kirby (1997).

In this case also, the fixed grid model predictions are closer to the predictions by Özkan Haller and Kirby (1997) than by Zelt (1986). It can also be noticed by comparing Figure 6.15 and 6.30 that the results with the fixed grid implementation of the moving shoreline have some minor wiggles in the surface elevation at the shoreline that were not present in the results with the coordinate transformation method. It may be attributed to the fact that with the fixed grids and a wet-dry interface, at a given time step the Shapiro filter, which is applied to remove the high frequency spurious oscillations, is applied only to grid points which were wet at that

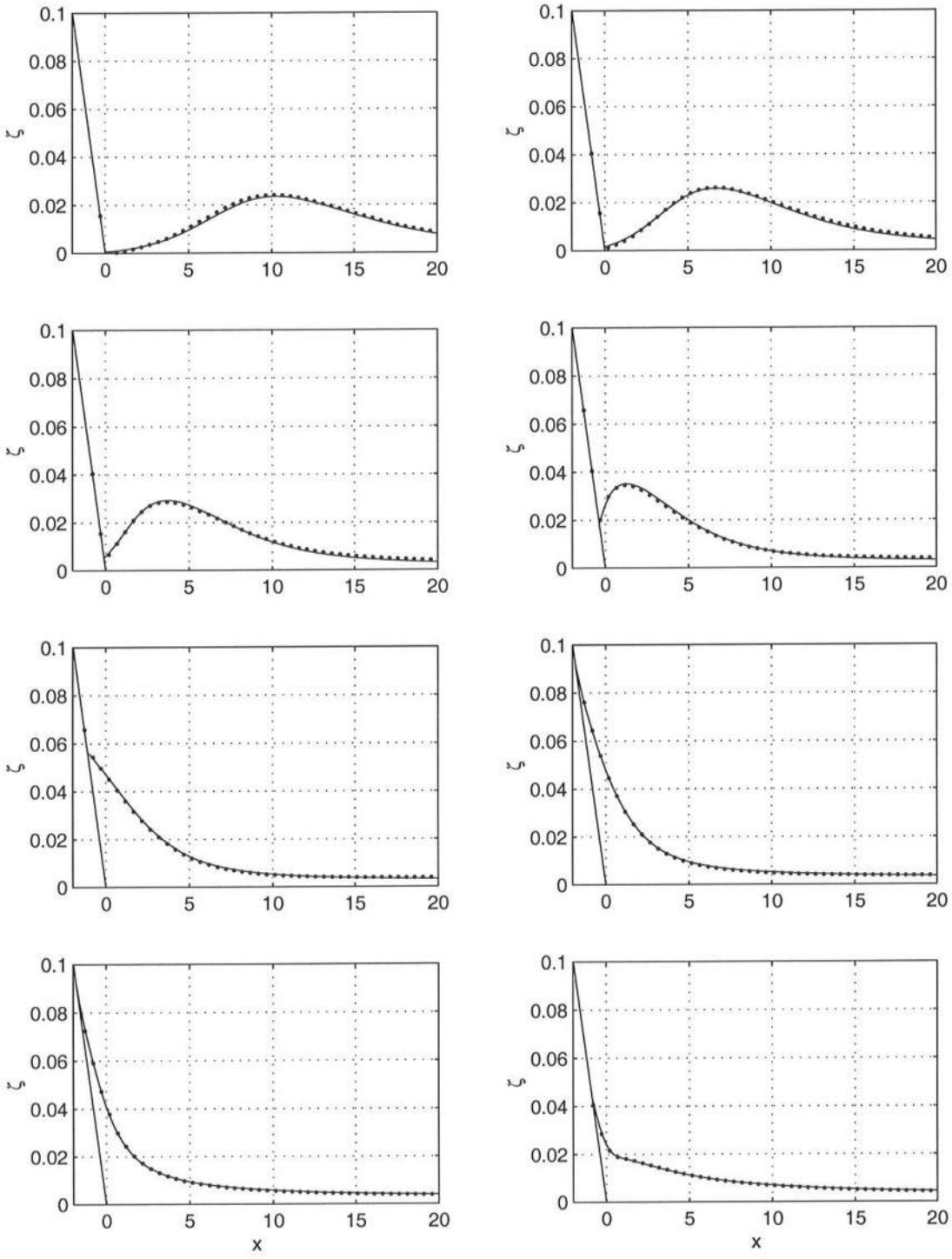

Figure 6.26: Run up of a solitary wave . The analytical solution (- - -); SHORE-CIRC with fixed grid (———).

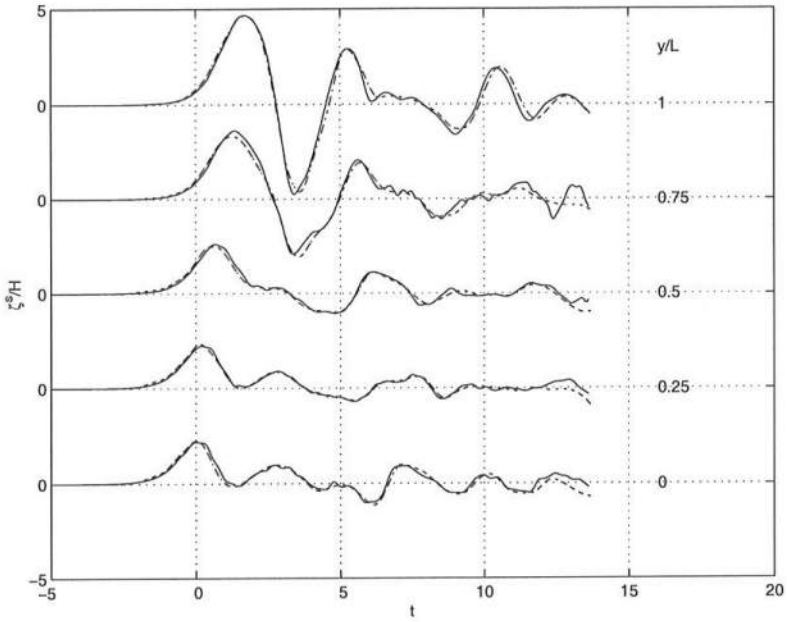

Figure 6.27: Time series of the surface elevation at the shoreline. SHORECIRC with fixed grid (———); Zelt (1986)(– · – · –).

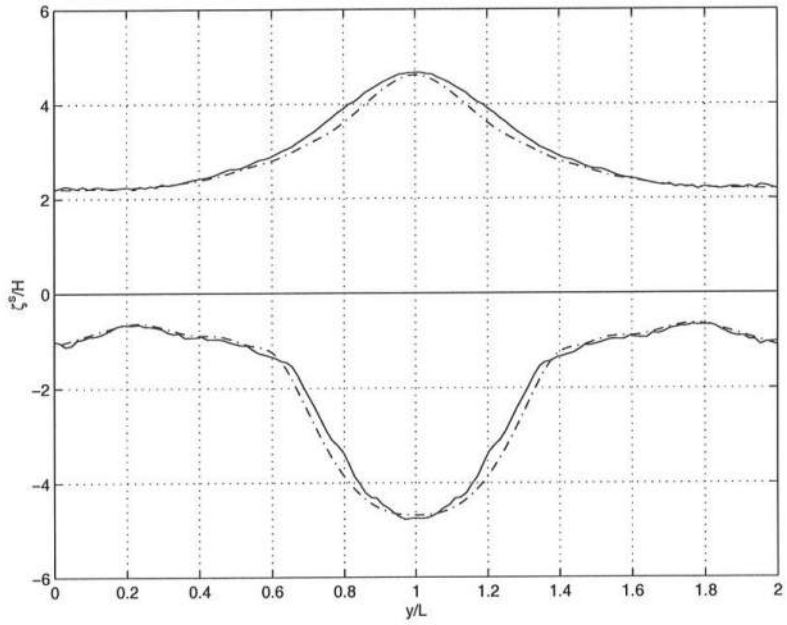

Figure 6.28: The maximum run-up and the minimum run-down as a function of the longshore position. SHORECIRC with fixed grids (———); Zelt (1986) (– · – · –).

instant of time. The shoreline points, which by definition, are always between the last wet and the first dry grid point, are never included in the filter scheme. In contrast, for the coordinate transformation scheme the shapiro filter can be used at all points at all time. This, however, does not change the fact that the agreement between the three methods is remarkably good.

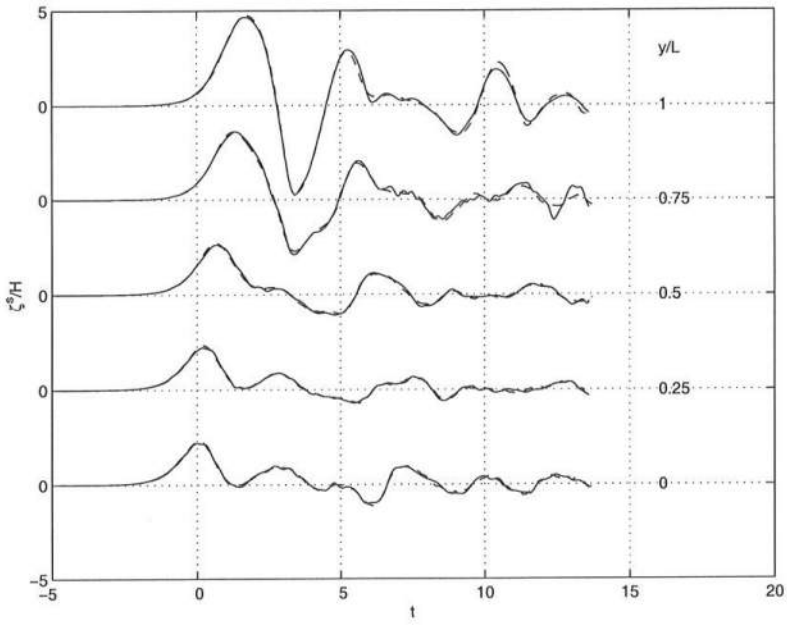

Figure 6.29: Time series of the surface elevation at the shoreline. SHORECIRC with fixed grids (———); Özkan Haller and Kirby (1997) (– – –).

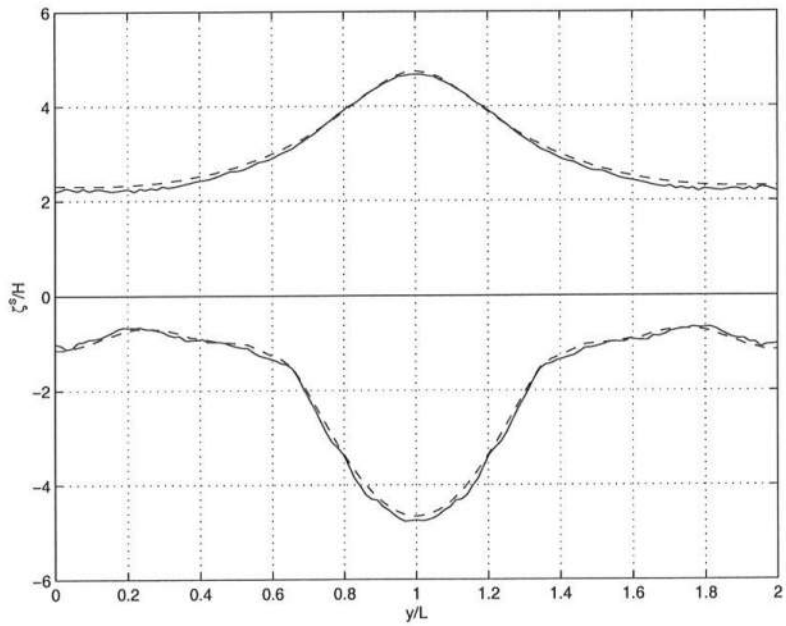

Figure 6.30: The maximum run-up and the minimum run-down. SHORECIRC with fixed grids (———); Özkan Haller and Kirby (1997) (– – –).

Chapter 7

SUMMARY AND CONCLUSIONS

7.1 Summary

In the present work the equations for the velocity of the shoreline have been derived. Two methods to incorporate the time variation of the fluid domain in a numerical model have been developed, one using a co-ordinate transformation and the other one with a wet-dry interface using a fixed grid. These methods have been implemented in the nearshore circulation model SHORECIRC and the results are compared with analytical results in one dimension and with numerical results in two horizontal directions.

For the co-ordinate transformation method, the actual time varying fluid domain was transformed onto a fixed computational domain. The transformation was chosen such that the instantaneous shoreline is mapped onto a fixed and straight line in the transformed plane and the evenly spaced grid points in the computational domain correspond to a smaller grid spacing near the shoreline than the grid spacing offshore.

The moving shoreline boundary condition has also been implemented by using a fixed grid and a wet-dry interface. The shoreline points, which in general lie between two grid points are treated as special points between regular grid point. When a shoreline point crosses a dry point during run-up, that point is declared wet and included in the computation. Similarly, when a shoreline point crosses a wet point during run-down, that point is declared dry and excluded from computation in following time steps.

The results presented here were obtained with the reduced SHORECIRC equations where short waves were not present and frictional dissipation and quasi 3D dispersion terms were neglected.

7.2 Conclusions

In the coordinate transformation method, the computational domain is fixed and has a rectangular grid. However the governing equations get modified and become more complex. Since a computational grid in this method corresponds to different points in the physical domain at different times, the time series of any flow property at a fixed position in the physical domain can't be obtained without an interpolation of the results, except at the shoreline and the offshore boundary which are always mapped to a fixed point in the computational domain.

With the fixed grid method, the governing equation remain unchanged. However, the model domain can become complex. This method results in a non-constant grid spacing between the last wet point and the shoreline position which requires new finite difference formulae there. The time series of flow properties are readily available with this method. With this method, Shapiro filter can not be applied up to the shoreline. This seems to be the reason for the small wiggles in the two dimensional case.

The comparison of the results with the co-ordinate transformation and the results with the wet-dry interface using fixed grid shows that when the grid spacing near the shoreline is same in these two methods, the accuracy of the results are comparable. The fact that far offshore, the grid spacing with the co-ordinate transformation method is much larger than that with fixed grid method does not introduce much error in the solution. The results with both the methods of inclusion of the time varying model domain reveal that the change in the grid spacing has a stronger effect on the solution than changes in the time step.

It was found out that the wet-dry method for the treatment of the moving shoreline is equally accurate as the co-ordinate transformation method as long as the grid spacing near the shoreline is same in both the cases. The co-ordinate transformation can be used to obtain a smaller grid spacing near the shoreline than the rest of the domain however, with the fixed grid method, the resolution in the offshore region is same as near the shoreline. This results in a high accuracy with co-ordinate transformation method for a lesser computational cost than that with the fixed grid method. However in the cases where a predominant shoreline doesn't exist e.g. bays and embayments, a transformation method may not be well suited.

In the present work the cases where short waves are not present are discussed. To include the effects of short wave motion, with the transformation method, a short wave driver is required which can provide radiation stresses and wave volume fluxes due to the short waves along the transformed grids. Non availability of such a wave driver may serve as one limitation on the transformation method to extend them to field situations. Whereas extension of the fixed grid method to field situations becomes fairly straightforward if the short wave properties are provided at different time steps as described by Haas and Svendsen (2000) using wave-current interaction.

ACKNOWLEDGMENTS

This work is a result of research sponsored by grant no N00014-97-1-0791 funded by the collaborative NICOP program and from the ONR grant N0014-99-1-0291. The U.S. Government is authorized to produce and distribute reprints for government purposes notwithstanding any copyright notation that may appear herein.

We would like to thank D. H. Peregrine, M. Brocchini, K. Haas, Q. Zhao, Q. Chen and F. Shi for many useful discussions during the course of this work.

Bibliography

Anderson, D. A., Tannehill, J. C., and Pletcher, R. H. (1984). *Computational fluid mechanics and heat transfer*. Series in computational methods in mechanical and thermal sciences. Hemisphere Publishing Corporation.

Balzano, A. (1998). Evaluation of methods for numerical simulation of wetting and drying in shallow water flow models. *Coastal engineering*, **34**, 83–107.

Brocchini, M. and Peregrine, D. H. (1996). Integral flow properties of the swash zone and averaging. *Journal of Fluid Mechanics*, **317**, 241–273.

Carrier, G. F. and Greenspan, H. P. (1958). Water waves of finite amplitude on a sloping beach. *Journal of Fluid Mechanics*, **4**(1), 97–109.

Gopalakrishnan, T. C. and Tung, C. C. (1983). Numerical analysis of a moving boundary problem in coastal hydrodynamics. *International Journal of Numerical Methods in Fluids*, **3**, 179–200.

Haas, K. and Svendsen, I. A. (2000). Three dimensional modeling of rip current system. Research Report CACR-00-06, University of Delaware.

Hibberd, S. and Peregrine, D. H. (1979). Surf and run-up on a beach: a uniform bore. *Journal of Fluid Mechanics*, **95**(2), 323–345.

Jamet, P. and Bonnerot, R. (1975). Numerical solution of the eulerian equations of compressible flow by finite element method which follows the free boundary and the interfaces. *Journal of Computational Physics*, **18**, 21–45.

Johns, B. (1982). Numerical integration of the shallow water equations over a sloping shelf. *International Journal for Numerical Methods in Fluids*, **2**, 253–261.

Johns, B., Dube, S. K., Sinha, P. C., Mohanty, U. C., and Rao, A. D. (1982). The simulation of a continuously deforming lateral boundary in problems involving the shallow water equations. *Computers and Fluids*, **10**(2), 105–116.

Kobayashi, N., Otta, A. K., and Roy, I. (1987). Wave reflection and run-up on rough slopes. *Journal of Waterways, Port, Coastal and Ocean Engineering*, **113**(3), 282–298.

Liu, P. L.-F., Cho, Y.-S., Briggs, M. J., Lu, U. K., and Synolakis, C. E. (1995). Runup of solitary waves on a circular island. *Journal of Fluid Mechanics*, **302**, 259–285.

Lynch, D. R. and Gray, W. G. (1980). Finite element simulation of flow in deforming regions. *Journal of Computational Physics*, **36**, 135–153.

Militello, A. (1998). *Hydrodynamics of Wind-Dominated, Shallow Embayments.* Ph.D. thesis, Florida Institute of Technology.

Özkan Haller, H. T. and Kirby, J. T. (1997). Nonlinear evolution of the shear instabilities of the longshore current. Research Report CACR 97-08, University of Delaware.

Pedersen, G. and Gjevik, B. (1983). Run-up of solitary waves. *Journal of Fluid Mechanics*, **135**, 283–299.

Putrevu, U. and Svendsen, I. A. (1991). Wave induced nearshore currents: A study of the forcing, mixing and stability characteristics. Research Report CACR-91-11, University of Delaware.

Putrevu, U. and Svendsen, I. A. (1994). Nearshore mixing and dispersion. Research Report CACR-94-08, University of Delaware.

Reid, R. O. and Bodine, B. R. (1968). Numerical model for storm surges in galveston bay. *Journal of the Waterways and Harbors Division*, **94**(WW 1), 33–57.

Sancho, F. and Svendsen, I. A. (1997a). Unsteady nearshore currents on longshore varying topographies. Research Report CACR-97-10, University of Delaware.

Shapiro, R. (1970). Smoothing, filtering and boundary effects. *Reviews of Geophysics and Space Physics*, **8**, 359–387.

Shi, F. and Sun, W. (1995). A variable boundary model of storm surge flooding in generalized curvilinear grids. *International Journal for Numerical Methods in Fluids*, **21**, 641–651.

Sielecki, A. and Wurtele, M. G. (1970). The numerical integration of the nonlinear shallow water equations with sloping boundaries. *Journal of Computational Physics*, **6**, 219–236.

Stoker, J. J. (1948). The formation of breakers and bores. *Communications on Pure and Applied Mathematics*, **1**, 1–80.

Synolakis, C. E. (1987). The runup of solitary waves. *Journal of Fluid Mechanics*, **185**, 523–545.

VanDongeren, A. R. and Svendsen, I. A. (1997a). An absorbing-generating boundary condition for shallow water models. *Journal of Waterway, port, coastal and Ocean Engg.*, **123**(6), 303–313.

VanDongeren, A. R. and Svendsen, I. A. (1997b). Quasi 3-d modeling of nearshore hydrodynamics. Research Report CACR-97-04, University of Delaware.

VanDongeren, A. R. and Svendsen, I. A. (2000). Nonlinear and 3D effects in leaky infragravity waves. *Coastal Engg.*, **123**(6), 303–313.

Zelt, J. A. (1986). Tsunamis: The response of harbours with sloping boundaries to long wave excitation. Technical Report KH-R-47, California Institute of Technology, Pasadena, California.

Zelt, J. A. (1991). The run-up of nonbreaking and breaking solitary waves. *Coastal Engineering*, **15**, 205–246.

Zelt, J. A. and Raichlen, F. (1990). A lagrangian model for wave induced harbor oscillation. *Journal of Fluid Mechanics*, **213**, 203–225.

Appendix A

THE CARRIER AND GREENSPAN SOLUTION

A.1 Introduction

Carrier and Greenspan (1958) presented an analytical solution of the Non-linear Shallow Water Equations. It shows that the waves can reach the shoreline without breaking. It also shows that whether or not a wave will break before it reaches the shoreline depends on the initial conditions of the wave. However, it doesn't determine a simple criterion under which a wave will break when it reaches the shoreline. In order to obtain the analytical results, it uses some transformations of the independent variables. In this chapter the transformations used, the results obtained by Carrier and Greenspan (1958) and how they were used in the present work to compare the model results will be described.

A.2 Transformation method

The NSW equations for one dimensional case are given by,

$$\zeta_t + [u(\zeta + h)]_x = 0, \tag{A.1}$$

$$u_t + uu_x + g\zeta_x = 0. \tag{A.2}$$

Where u is the depth averaged velocity, ζ the surface elevation, h the undisturbed waterdepth, x the cross-shore position and t is time. By using the scaling, given by (6.5), (6.6), (6.7), and (6.8) along with $c^{*2} = (h + \zeta)/h_x L$ and $h = -h_x x$, A.1 and A.2 arrive at their non-dimensional form as,

$$u^*_{t^*} + u^* u^*_{x^*} + \zeta^*_{x^*} = 0. \tag{A.3}$$

$$\zeta^*_{t^*} + [u^*(\zeta^* - x^*)]_{x^*} = 0 \tag{A.4}$$

For simplicity, superscript (*) has been omitted from now on. In the following all the variables are in the non-dimensional form unless otherwise stated.

On replacing ζ by c using the relation for the phase speed in the non-dimensional form $c = \sqrt{\zeta - x}$, in (A.3) and (A.4) and adding and subtracting them as described by Stoker (1948), we get,

$$\left(\frac{\partial}{\partial t} + (u+c)\frac{\partial}{\partial x}\right)\{u + 2c + t\} = 0 \tag{A.5}$$

$$\left(\frac{\partial}{\partial t} + (u-c)\frac{\partial}{\partial x}\right)\{u - 2c + t\} = 0 \tag{A.6}$$

On defining α and β such that,

$$\left(\frac{\partial}{\partial t} + (u+c)\frac{\partial}{\partial x}\right) = \frac{\partial}{\partial \beta} \tag{A.7}$$

$$\left(\frac{\partial}{\partial t} + (u-c)\frac{\partial}{\partial x}\right) = \frac{\partial}{\partial \alpha} \tag{A.8}$$

equations (A.5) and (A.6) reduce to,

$$u_\beta + 2c_\beta + t_\beta = 0 \tag{A.9}$$

$$u_\alpha - 2c_\alpha + t_\alpha = 0 \tag{A.10}$$

On applying the differential operator $\partial/\partial\beta$ from (A.7) on x and t we get,

$$x_\beta = u + c \tag{A.11}$$

$$t_\beta = 1 \tag{A.12}$$

This can be rearranged such that,

$$x_\beta - (u+c)t_\beta = 0 \tag{A.13}$$

Similarly by applying the differential operator $\partial/\partial\alpha$ from (A.8) on x and t we will get,

$$x_\alpha - (u-c)t_\alpha = 0 \tag{A.14}$$

The variables α and β here are treated as the independent variables and u, ζ, x and t as their unknown functions.

The LHS of equations (A.9) and (A.10) are exact differentials, so they can be integrated directly. Which gives,

$$u + 2c + t = f(\alpha), \tag{A.15}$$

$$u - 2c + t = g(\beta). \tag{A.16}$$

Here f and g are any arbitrary functions of α and β respectively.

The equations (A.15) and (A.16) can be rearranged such that,

$$2(u + t) = f(\alpha) + g(\beta) = \lambda, \tag{A.17}$$

$$4c = f(\alpha) - g(\beta) = \sigma. \tag{A.18}$$

The equations (A.17) and (A.18) define λ and σ respectively, which are then chosen as the final set of independent variables. Since σ and λ are the independent variables now, the derivatives with respect to α and β need to be changed to those with respect to σ and λ. This transformation can be obtained by successive differentiation and is given by,

$$\frac{\partial}{\partial \alpha} = \frac{\partial}{\partial \sigma}\sigma_\alpha + \frac{\partial}{\partial \lambda}\lambda_\alpha \tag{A.19}$$

$$\frac{\partial}{\partial \beta} = \frac{\partial}{\partial \sigma}\sigma_\beta + \frac{\partial}{\partial \lambda}\lambda_\beta \tag{A.20}$$

From equations (A.17) and (A.18),

$$\sigma_\alpha = f'(\alpha) \qquad \sigma_\beta = -g'(\beta) \tag{A.21}$$

$$\lambda_\alpha = f'(\alpha) \qquad \lambda_\beta = g'(\beta) \tag{A.22}$$

On substituting the values of σ_α, σ_β, λ_α and λ_β from (A.21) and (A.22) into (A.19) and (A.20) we get,

$$\frac{\partial}{\partial \alpha} = f'(\alpha)\left(\frac{\partial}{\partial \sigma} + \frac{\partial}{\partial \lambda}\right) \tag{A.23}$$

$$\frac{\partial}{\partial \beta} = -g'(\beta)\left(\frac{\partial}{\partial \sigma} - \frac{\partial}{\partial \lambda}\right) \tag{A.24}$$

When (A.23) and (A.24) are substituted in (A.13) and (A.14), we get,

$$-g'(\beta)\left[(x_\sigma - x_\lambda) - (u+c)(t_\sigma - t_\lambda)\right] = 0 \tag{A.25}$$

$$f'(\alpha)\left[(x_\sigma + x_\lambda) - (u-c)(t_\sigma + t_\lambda)\right] = 0 \tag{A.26}$$

$f'(\alpha) = 0$ and $g'(\beta) = 0$ imply that $f(\alpha)$ and $g(\beta)$ are constant and this along with (A.15) and (A.16) implies that c and thus the waterdepth is constant. So the non-trivial solution of (A.25) and (A.26) are given by,

$$(x_\sigma - x_\lambda) - (u+c)(t_\sigma - t_\lambda) = 0 \tag{A.27}$$

$$(x_\sigma + x_\lambda) - (u-c)(t_\sigma + t_\lambda) = 0. \tag{A.28}$$

The equations (A.27) and (A.28) can be rearranged to yield,

$$x_\sigma - ut_\sigma + ct_\lambda = 0, \tag{A.29}$$

$$x_\lambda + ct_\sigma - ut_\lambda = 0. \tag{A.30}$$

Now x can be eliminated from (A.29) and (A.30) by differentiating (A.29) with respect to λ and (A.30) with respect to σ. This results in a single equation for t which is given by,

$$c(t_{\lambda\lambda} - t_{\sigma\sigma}) - (u_\lambda + c_\sigma)t_\sigma + (c_\lambda + u_\sigma)t_\lambda = 0 \tag{A.31}$$

From (A.18),

$$c_\lambda = 0 \qquad \text{and} \qquad c_\sigma = \frac{1}{4} \tag{A.32}$$

and from (A.17)

$$u_\lambda + t_\lambda = \frac{1}{2} \qquad \text{and} \qquad u_\sigma = t_\sigma \tag{A.33}$$

On substitution from the expressions above, (A.31) simplifies to,

$$c(t_{\lambda\lambda} - t_{\sigma\sigma}) - \frac{3}{4}t_\sigma = 0 \tag{A.34}$$

or,

$$\sigma(t_{\lambda\lambda} - t_{\sigma\sigma}) - 3t_\sigma = 0 \tag{A.35}$$

From (A.17),

$$u_\sigma = -t_\sigma \tag{A.36}$$

$$u_{\sigma\sigma} = -t_{\sigma\sigma} \tag{A.37}$$

and $$u_{\lambda\lambda} = -t_{\lambda\lambda} \tag{A.38}$$

On substituting these into (A.35) we get,

$$\sigma(u_{\lambda\lambda} - u_{\sigma\sigma}) - 3u_\sigma = 0 \tag{A.39}$$

On introducing a potential function $\phi(\sigma, \lambda)$ such that,

$$u = \frac{\phi_\sigma}{\sigma} \tag{A.40}$$

(A.39) reduces to

$$(\sigma\phi_\sigma)_\sigma - \sigma\phi_{\lambda\lambda} = 0 \tag{A.41}$$

and, (A.17), (A.18) and (A.29) gives,

$$t = \frac{\lambda}{2} - u \tag{A.42}$$

$$\zeta = \frac{\phi_\lambda}{4} - \frac{u^2}{2} \tag{A.43}$$

$$x = \frac{\phi_\lambda}{4} - \frac{\sigma^2}{16} - \frac{u^2}{2} \tag{A.44}$$

With these transformations, the nonlinear equations have been transformed in a linear equation. The moving shoreline position has been mapped to $\sigma = 0$ in the transformed plane. The surface elevation, the velocity, the offshore distance and time are obtained as explicit function of the independent variables σ and λ.

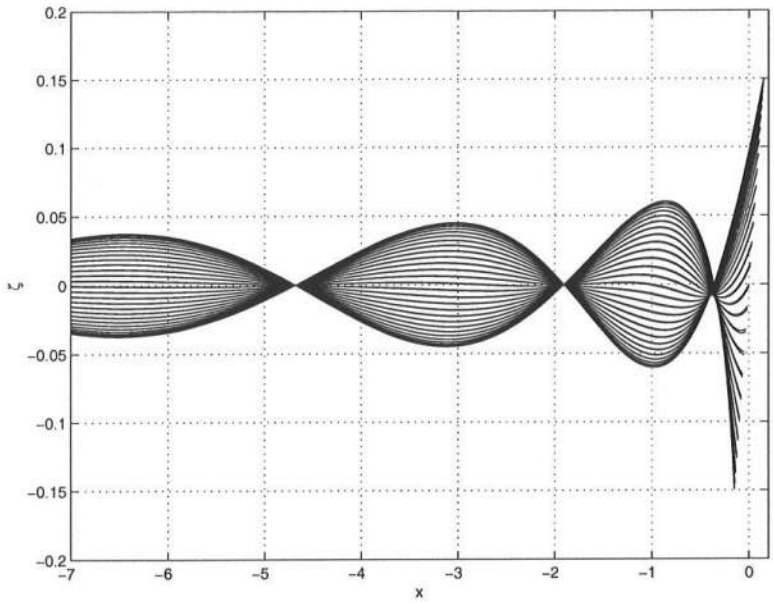

Figure A.1: Carrier and Greenspan solution for surface elevation as a function of cross-shore distance at different times.

A.3 Periodic case and it's solution

One of the solutions of (A.41) is,

$$\phi(\sigma, \lambda) = AJ_0(\sigma) \sin \lambda \tag{A.45}$$

This results in,

$$u = \frac{AJ_1(\sigma) \sin \lambda}{\sigma} \tag{A.46}$$

$$x = \frac{AJ_0(\sigma) \cos \lambda}{4} - \frac{\sigma^2}{16} - \frac{(AJ_1(\sigma) \sin \lambda)^2}{2\sigma^2} \tag{A.47}$$

$$\zeta = \frac{AJ_0(\sigma) \cos \lambda}{4} - \frac{(AJ_1(\sigma) \sin \lambda)^2}{2\sigma^2} \tag{A.48}$$

$$t = \frac{\lambda}{2} - \frac{AJ_1(\sigma) \sin \lambda}{\sigma} \tag{A.49}$$

This represents the case of full reflection of an incoming wave from the shoreline and forming a standing wave. Figure A.1 and A.2 shows the surface elevation and the velocity profile respectively for $A = 0.6$ as a function of the cross-shore distance x at different time t.

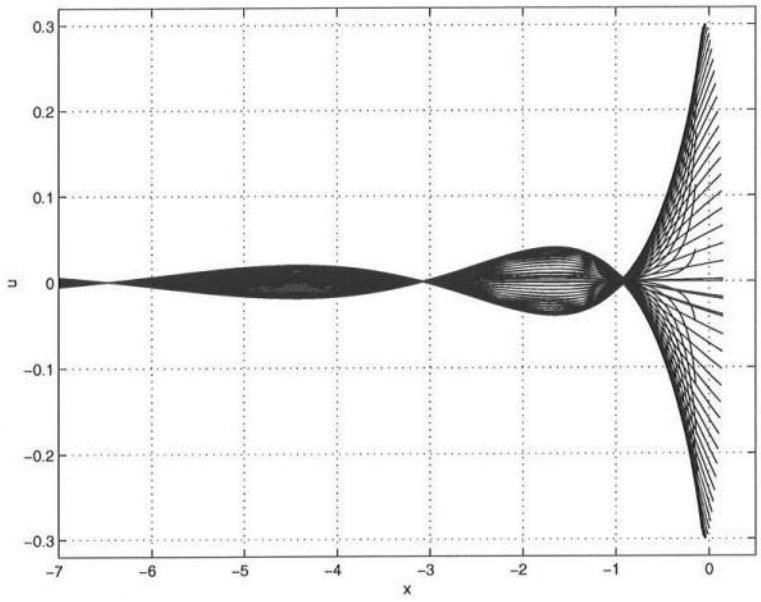

Figure A.2: Carrier and Greenspan solution for velocity as a function of cross-shore distance at different times.

A.4 Transient case and it's solution

Some cases of the response of the release of a fixed initial shape of the water surface elevation had been discussed by CG58. In one of these cases, the initial waveform was given by a one parameter family of curves,

$$\zeta = \epsilon\left[1 - \frac{5}{2}\frac{a^3}{(a^2+\sigma^2)^{\frac{3}{2}}} + \frac{3}{2}\frac{a^5}{(a^2+\sigma^2)^{\frac{5}{2}}}\right] \tag{A.50}$$

$$x = -\frac{\sigma^2}{16} + \zeta \tag{A.51}$$

where, $a = 1.5(1+0.9\epsilon)^{1/2}$ and ϵ is the small parameter.

This represent the case where a mound of water with a depression near the shoreline is released from the state of rest at time $t = 0$. The solution for this case is given by,

$$u = \frac{8\epsilon}{a}\Im\left\{\frac{1}{\{(1-i\lambda)^2+\sigma^2\}^{3/2}} - \frac{3}{4}\frac{1-i\lambda}{\{(1-i\lambda)^2+\sigma^2\}^{5/2}}\right\}, \tag{A.52}$$

$$\phi = 8\epsilon a\Im\left\{\frac{-1}{\{(1-i\lambda)^2+\sigma^2\}^{1/2}} + \frac{1}{4}\frac{1-i\lambda}{\{(1-i\lambda)^2+\sigma^2\}^{3/2}}\right\}, \tag{A.53}$$

$$x = -\frac{u^2}{2} - \frac{a^2\sigma^2}{16} + \frac{\phi_\lambda}{4}, \tag{A.54}$$

$$t = \frac{a\lambda}{2} - u, \tag{A.55}$$

$$\zeta = x + \frac{a^2\sigma^2}{16}. \tag{A.56}$$

Here σ and λ have been replaced by $a\sigma$ and $a\lambda$ respectively.

A.5 Solutions for fixed x and t

The solutions described above are given as $u(\sigma, \lambda)$, $\zeta(\sigma, \lambda)$, $x(\sigma, \lambda)$ and $t(\sigma, \lambda)$. Since most of the numerical models solve the governing equations along fixed x and for constant time step, it's needed here to obtain a suitable method to transform these back for constant x and t before it could be used to compare the results of the numerical simulations. This is done here by finding σ and λ such that dx is constant and $dt = 0$. dx and dt are given by,

$$dt = \frac{\partial t}{\partial \sigma} d\sigma + \frac{\partial t}{\partial \lambda} d\lambda \tag{A.57}$$

$$dx = \frac{\partial x}{\partial \sigma} d\sigma + \frac{\partial x}{\partial \lambda} d\lambda \tag{A.58}$$

$dt = 0$ results in,

$$d\lambda = -\left(\frac{\partial t}{\partial \sigma}\right) / \left(\frac{\partial t}{\partial \lambda}\right) d\sigma \tag{A.59}$$

On substituting from (A.59) to (A.58) we get,

$$dx = \left[\frac{\partial x}{\partial \sigma} - \left(\frac{\frac{\partial t}{\partial \sigma}}{\frac{\partial t}{\partial \lambda}}\right) \frac{\partial x}{\partial \lambda}\right] d\sigma \tag{A.60}$$

Equations (A.60) and (A.59) can be used to find $d\sigma$ and $d\lambda$ at a constant time when a constant dx has been specified. However, the first point known at any time is at $\sigma = 0$ and for the periodic case, co-efficient of $d\sigma$ in (A.60) becomes zero at $\sigma = 0$. So, instead a constant $d\sigma$ has been specified and value of x is calculated from (A.60).

For any time t, $\lambda(\sigma = 0, t)$ is calculated from (A.42). Initial surface elevation ζ is used to specify the initial condition in the numerical model whereas at other t values it's used to compare the result of the simulations.